Applying Interpolation Techniques to Search for Transonic Aeroelastic Instability: ANN vs Kriging

S. Timme*, A. Rampurawala† and K. J. Badcock‡

CFD Laboratory, University of Liverpool, Liverpool L63 3GH, United Kingdom

Interpolation techniques including artificial neural networks and kriging are applied to predict transonic aeroelastic instability in larger parameter spaces for aerofoil and wing configurations. The linear stability problem is formulated as a small structural eigenvalue problem corrected by the aerodynamic influence which is given by the interaction matrix and modelled by nonlinear computational fluid dynamics using the Euler equations. The evaluation of the interaction matrix depending on the response frequency and the steady state solution incurs most of the involved computational cost as it requires operations on the large fluid system, and hence its approximation is required for routine calculations. The approximation is done by interpolation based on exact numerical samples which can be evaluated in either the frequency or time domain. The general applicability of the interpolation techniques for the analyses is discussed and the approximation models are exploited for blind search of aeroelastic instability.

1. Introduction

Aircraft aeroelasticity deals with the mutual interaction of aerodynamic, elastic, and inertial forces for a flexible structure. The resulting aeroelastic phenomena are safety–related and have played an important role since the beginning of modern aircraft [1]. The flutter phenomenon is one of the most important examples as this violent unstable structural vibration, usually originating in the coupling of two vibrational modes, potentially leads to catastrophic structural failure. Aerodynamic and/or structural nonlinearities make an aeroelastic system susceptible to bounded flutter responses which are commonly referred to as limit–cycle oscillations or limit–cycle flutter [2]. The aerodynamics in the transonic regime, featuring shock waves and shock induced separation, are a major source of nonlinearity, and a careful modelling of the flow field is required to predict aeroelastic instability accurately. However, the nonlinear transonic aerodynamics are the most difficult to model numerically and experimentally [3]. As modern aircraft operate routinely in the transonic regime, a considerable effort has been made towards the improvement of current analysis capabilities. In this work we mostly assume dynamically linear systems and the prediction of the linear aeroelastic stability limit is the main concern. This means that the steady state flow field may exhibit nonlinear flow phenomena, such as shock waves and separation, while the dynamic response is time–linearised about the nonlinear steady state solution assuming there is a linear relationship between the structural motion and the fluid response. The structural representation is considered to be linear throughout.

The fast prediction and understanding of aeroelastic instability, particularly in the transonic regime, is an important task in modern aircraft design. Standard approaches in industrial applications to determine the stability of an aircraft structure are the k or p–k methods [4]. These assume an inviscid linearised theory in the frequency domain for the unsteady aerodynamic response. Most notably the doublet lattice method has been the single most important tool in large scale production flutter analyses for more than 30

*Research Associate, School of Engineering. email: Sebastian.Timme@liverpool.ac.uk

†Honorary Research Associate, School of Engineering.

‡Professor, School of Engineering. email: K.J.Badcock@liverpool.ac.uk

years [5]. However, for the important transonic regime with its mixed sub- and supersonic regions, a linear aerodynamic theory fails due to the presence of flow nonlinearities including shock waves and shock induced flow separation, and the linear numerical predictions have to be corrected with data from expensive and time–consuming experimental campaigns or higher fidelity flow simulations.

Inferring the stability of an aeroelastic system from time–accurate simulations is very capable due to its generality. However, the significant computational cost, in particular to solve for the unsteady, nonlinear transonic aerodynamics, is a major drawback of this approach which is emphasised by the requirement to search parameter spaces for critical conditions. To obviate the cost involved in solving complex systems with millions of degrees–of–freedom, and to permit routine calculations over the flight envelope, alternative approaches have been investigated over the last decade. There are two distinct directions. One, referred to as reduced order modelling, extracts the essence of the dynamic aeroelastic system to form a low dimensional problem while trying to keep the accuracy of the full order formulation. Popular approaches are system identification based on the Volterra theory [6, 7] and proper orthogonal decomposition [8–10]. The second direction keeps the order of the full system while manipulating its solution procedure to reduce the cost. One method, based on dynamical system theory, predicts aeroelastic instability of the Hopf type, commonly leading to flutter or limit–cycle oscillations, from a steady state solution of the system.

Following an approach first published in [11–13], the bifurcation method, solving an augmented system of equations for the bifurcation point, was successfully tested on an aerofoil configuration free to move in pitch and plunge. Convergence problems associated with applying a direct solver to a large linear system were resolved by using an iterative sparse linear solver [14]. The method was extended to a larger problem investigating the flexible AGARD 445.6 wing using a modal structural model [15]. However, the aeroelastic system using computational fluid dynamics (CFD) is typically large making it difficult to solve the augmented system for the bifurcation point directly. Thus, three major development steps have taken place since this early work.

First, the shifted inverse power method was adapted to allow the tracing of the critical eigenvalues, typically emerging from the wind–off structural system, with changing values of the independent system parameter (i.e. a representation of the dynamic pressure) to provide information about the damping and frequency of the aeroelastic modes [16].

Secondly, an improved version of the basic method used a Schur complement eigenvalue formulation to enhance computational performance and to avoid numerical problems associated with the shifted inverse power method [17]. It was applied to several wing structures and also complete aircraft configurations to study uncertainty in the predicted instability due to structural variability [18]. This approach views the coupled aeroelastic system as a modified structural eigenvalue problem with the interaction (correction) term, which depends on the response frequency, pre–computed. The evaluation of the interaction term incurs most of the involved cost as it generally requires operations on the high dimensional CFD–based system.

Thirdly, the approximation of this interaction term was formulated both to search parameter spaces for aeroelastic instability and to exploit a hierarchy of nonlinear aerodynamic models, with cheaper models being used to evaluate possible conditions of interest for more expensive models, whose evaluation is then used to update the approximation [19, 20]. The approximation of the interaction term using kriging interpolation made the Schur method for aeroelastic stability analysis essentially a reduced order model.

In this paper an alternative to the kriging interpolation is discussed. Artificial neural networks are tested and compared to the previous results from the kriging–based approach. In Sections 2 and 3 the aerodynamic and structural models and the tools required for the aeroelastic stability analysis are described. In Section 4 the general applicability of the approximations for the stability analysis using both kriging and artificial neural networks is presented. The approach of coordinated risk–based sampling is analysed in Section 5 to search for aeroelastic instability at reduced computational cost.

2. Governing Equations of the Flow and Structure

A. Flow Model

In the current paper, the Euler equations are used as the aerodynamic model. These equations are solved using an established research code [21]. The code uses a block–structured, cell–centred, finite–volume scheme

for spatial discretisation. Convective fluxes are evaluated by the approximate Riemann solver of Osher and Chakravarthy [22] with the MUSCL scheme [23] achieving essentially second order accuracy and van Albada's limiter preventing spurious oscillations around steep gradients. Boundary conditions are enforced using two layers of halo cells.

Spatial discretisation leads to a system of first order ordinary differential equations in time which can be written in semidiscrete state–space form as $\dot{\boldsymbol{w}}_f = \boldsymbol{R}_f(\boldsymbol{w})$, with $\boldsymbol{w}_f$ as the vector of fluid unknowns and $\boldsymbol{R}_f$ as the corresponding residual vector. The vector $\boldsymbol{w}$ of unknowns contains both fluid and structural contributions with the latter contribution due to the dependence of the fluid residual on the grid location and velocity. Implicit time marching converges to steady state solutions, while dual time stepping is used for unsteady simulations with a second order temporal discretisation [24]. Resulting linear systems are solved by a preconditioned Krylov subspace iterative method. Details can be found in [21].

B. Structural Model

Aerofoil Structural Model

The "typical section" aerofoil model, with oscillating pitching and plunging motions, represents the torsional and bending behaviour of a wing structure. The two degrees–of–freedom model is idealised as a point mass located at the centre of gravity (cg), as well as a torsional and translational spring attached to the elastic centre (ec) located a dimensionless distance $x_\alpha/2$ from the centre of gravity, where x_α is measured in semichords and negative for an elastic centre ahead of the centre of gravity. The aerofoil model is depicted in Fig. 1.

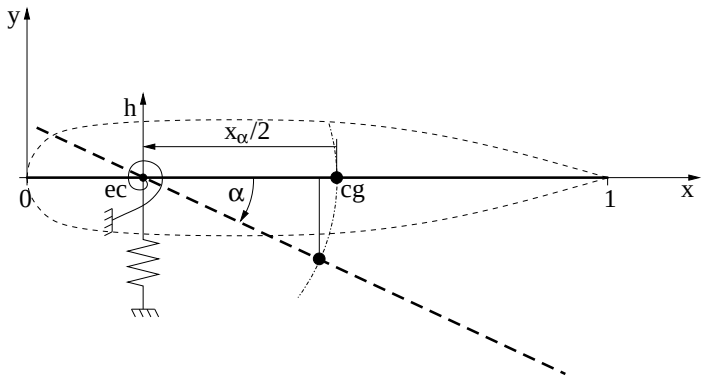

Figure 1. Depiction of two degrees–of–freedom aerofoil.

The linearised equations of motion are written in state–space representation as $\dot{\boldsymbol{w}}_s = \boldsymbol{R}_s(\boldsymbol{w})$, with $\boldsymbol{w}_s = [\,\boldsymbol{\eta}, \dot{\boldsymbol{\eta}}\,]^T$ containing the generalised coordinates of the two degrees–of–freedom and their corresponding velocities, and $\boldsymbol{w}$ contains both fluid and structural contributions. Ignoring structural damping, the residual vector is written as $\boldsymbol{R}_s = D\,\boldsymbol{w}_s + E\,\boldsymbol{f}(\boldsymbol{w})$, with the matrices $D = [0, I; -M^{-1}K, 0]$ and $E = [0, M^{-1}]^T$, where I is the 2×2 identity matrix. The vector of generalised forces $\boldsymbol{f}$ contains the integrated aerodynamic loads of lift and pitching moment about the elastic centre. The independent parameter for the aeroelastic simulations in the current paper is the reduced velocity $\bar{u}$, which is a dimensionless representation of the freestream velocity and only contained in the stiffness matrix K. Details about the aerofoil structural model are given in [14, 25].

The evaluation of the Jacobian matrix blocks is required for the eigenvalue–based stability analysis. Evaluating the structural Jacobian matrix A_{ss}, and the coupling block A_{sf}, is straightforward. The matrix block A_{ss} simply becomes $A_{ss} = D$. In this latter expression the dependence of the structural residual on the structural unknowns through the integrated aerodynamic loads, i.e. $E\,\partial \boldsymbol{f}/\partial \boldsymbol{w}_s$, is ignored. This contribution, which is due to changes in the surface normal vectors with changes in the structural unknowns at fixed flow solution, was found to be very small. The matrix block A_{sf} requires the dependence of the integrated loads on the fluid unknowns, $A_{sf} = E\,\partial \boldsymbol{f}/\partial \boldsymbol{w}_f$, which is evaluated by finite differences.

Modal Structural Model

The deflections $\delta\boldsymbol{x}_s$ of the structure are defined at a set of points $\boldsymbol{x}_s$ by $\delta\boldsymbol{x}_s(t) = \Phi(\boldsymbol{x}_s)\,\boldsymbol{\eta}(t)$, where the vector $\boldsymbol{\eta}$ contains the n generalised coordinates (modal amplitudes). This follows common practice in computational aeroelasticity [15, 26] by representing an aircraft structure by a small number of normal modes, small compared with the large dimension of the CFD system. The columns of the matrix Φ contain the mode shape vectors evaluated from a finite–element model of the structure using the commercial software package MSC.Nastran. The finite–element equations are projected onto the mode shapes and an appropriate scaling is applied to obtain generalised masses of magnitude one according to $\Phi^T M \Phi = I$. Using the trivial expression $\dot{\boldsymbol{\eta}} I = \dot{\boldsymbol{\eta}} I$, a system of $2n$ scalar equations is given for the modal structural model in state–space representation, denoted here as $\dot{\boldsymbol{w}}_s = \boldsymbol{R}_s(\boldsymbol{w})$, with the notation following the aerofoil structural model. The corresponding residual vector, neglecting structural damping, is written as $\boldsymbol{R}_s = D\,\boldsymbol{w}_s + \mu\,E\,\Phi^T\boldsymbol{f}(\boldsymbol{w})$, with the matrices $D = [0, I; -\Phi^T K \Phi, 0]$ and $E = [0, I]^T$, where I is the $n \times n$ identity matrix. The generalised stiffness matrix $\Phi^T K \Phi$ contains the n normal mode frequencies squared on the diagonal. The vector $\boldsymbol{f}$ of aerodynamic forces at the structural grid points is evaluated as the wall pressure times the area of the surface segment and the unit normal vector. The independent (bifurcation) parameter μ is calculated as (reference density)$\times$(reference length)^5. This relation follows from the nondimensionalisation of the governing equations.

The matrix A_{ss} is conveniently split into two contributions; one dominated by the normal mode frequencies and one due to the aerodynamic force vector. It is given by $A_{ss} = D + \mu\,E\,\Phi^T \partial\boldsymbol{f}/\partial\boldsymbol{w}_s$. The second term is usually negligible. The Jacobian matrix block A_{sf} is formed as $A_{sf} = \mu\,E\,\Phi^T \partial\boldsymbol{f}/\partial\boldsymbol{w}_f$. Currently, the evaluation of the derivatives $\partial\boldsymbol{f}/\partial\boldsymbol{w}_s$ and $\partial\boldsymbol{f}/\partial\boldsymbol{w}_f$ is done using finite differences. Conveniently, the bifurcation parameter is set to unity for the evaluation of the Jacobian matrices and adjusted in a matched fashion once needed as discussed in the following.

3. Eigenvalue Stability Formulation

A. Schur Complement Eigenvalue Method

Write the aeroelastic system in semidiscrete state–space form as $\dot{\boldsymbol{w}} = \boldsymbol{R}(\boldsymbol{w}, \mu)$, where the vector of unknowns $\boldsymbol{w} = [\boldsymbol{w}_f, \boldsymbol{w}_s]^T$ contains fluid and structural contributions, and $\boldsymbol{R}$ is the corresponding residual vector. The system depends on an independent parameter μ, typically representating the dynamic pressure. An equilibrium solution $\boldsymbol{w}_0$ of the nonlinear system satisfies $\boldsymbol{R}(\boldsymbol{w}_0, \mu) = 0$. The theory of dynamic systems gives criteria for an equilibrium to be stable. In particular, stability is determined by eigenvalues, $\lambda = \sigma \pm i\omega$, of the system Jacobian matrix $A(\boldsymbol{w}_0, \mu)$ evaluated at the steady state and chosen values of μ. A stable system has all its eigenvalues with a negative real part. In many aeroelastic problems a pair of complex conjugate eigenvalues with zero real part marks the onset of an instability of the Hopf type leading to flutter and limit–cycle oscillation.

Linear stability is predicted by solving the standard eigenvalue problem $(A - \lambda I)\,\boldsymbol{p} = 0$, where the Jacobian matrix A is conveniently partitioned in blocks expressing the different dependencies,

$$A = \frac{\partial \boldsymbol{R}}{\partial \boldsymbol{w}} = \begin{pmatrix} A_{ff} & A_{fs} \\ A_{sf} & A_{ss} \end{pmatrix}. \tag{1}$$

Importantly, the matrix A is the exact Jacobian matrix of the applied spatial discretisation scheme. Details about the evaluation of the Jacobian matrices can be found in [14–16].

Solving the full standard eigenvalue problem through shift and invert methods results in an increasingly ill–conditioned system as the converged eigenvalue is approached. To avoid this, the eigenvector $\boldsymbol{p}$ is partitioned into unknowns corresponding to fluid and structural contributions [17]. Then, the Schur complement eigenvalue problem is given as,

$$S(\lambda)\,\boldsymbol{p}_s = 0, \tag{2}$$

which is a small nonlinear eigenvalue problem of dimension $2n$ where n is the number of the structural degrees–of–freedom. The Schur complement matrix $S(\lambda)$ is explicitly written as,

$$S(\lambda) = (A_{ss} - \lambda I) - A_{sf}\,(A_{ff} - \lambda I)^{-1}\,(A_{f\eta} + \lambda\,A_{f\dot{\eta}}), \tag{3}$$

with the matrix $A_{fs} = [A_{f\eta}, A_{f\dot{\eta}}]$ rearranged to illustrate the dependence of the fluid residual $\boldsymbol{R}_f(\boldsymbol{w}_f, \boldsymbol{x}, \dot{\boldsymbol{x}})$ on the structural unknowns $\boldsymbol{w}_s = [\boldsymbol{\eta}, \dot{\boldsymbol{\eta}}]$ with generalised coordinates $\boldsymbol{\eta}$ (according to the structural degrees–of–freedom) and their velocities $\dot{\boldsymbol{\eta}}$ influencing the grid displacements $\boldsymbol{x}(\boldsymbol{\eta})$ and grid velocities $\dot{\boldsymbol{x}}(\dot{\boldsymbol{\eta}})$ of the fluid mesh. This relation can be seen by observing that for the state–space representation the structural eigenvector is written as $\boldsymbol{p}_s = [\boldsymbol{p}_\eta, \lambda\,\boldsymbol{p}_\eta]^T$ using the expression $\boldsymbol{\eta} = \boldsymbol{p}_\eta\, e^{\lambda t}$ consistent with a linear stability analysis [27].

In the Schur complement matrix, the first term on the right–hand side, $S^s = A_{ss} - \lambda I$, defines the structural eigenvalue problem, while the second part, $S^c = -A_{sf}\,(A_{ff} - \lambda I)^{-1}(A_{f\eta} + \lambda\, A_{f\dot{\eta}})$, constitutes the interaction term, the evaluation of which incurs most of the computational cost due to the large dimension of the fluid Jacobian matrix A_{ff}. Thus, the stability calculation is formulated as a modified structural eigenvalue problem corrected by the influence of the fluid system. As the interaction goes to zero, the structural eigenvalue problem is restored.

To solve the small complex–valued eigenvalue problem in Eq. (2), the system is augmented to scale the structural eigenvector $\boldsymbol{p}_s$ against an arbitrary real–valued constant vector $\boldsymbol{c}_s$ to produce a unique solution, i.e. augment by the (arbitrary) equation $\boldsymbol{c}_s^T \boldsymbol{p}_s = i$. Then, the augmented nonlinear system is solved for the unknowns $[\boldsymbol{p}_s, \lambda]^T$ using Newton–like methods as described in [17, 19]. There are n relevant solutions of the nonlinear eigenvalue problem. For convenience, a series approximation [28] of the Schur complement matrix can be written for $\lambda = \lambda_0 + \lambda_\varepsilon$ as,

$$S(\lambda) \approx (A_{ss} - \lambda I) - A_{sf} \left(\, (A_{ff} - \lambda_0 I)^{-1} + \lambda_\varepsilon (A_{ff} - \lambda_0 I)^{-2} \, \right) (A_{f\eta} + \lambda_0\, A_{f\dot{\eta}} + \lambda_\varepsilon\, A_{f\dot{\eta}}), \tag{4}$$

where λ_ε is a small variation to the reference value λ_0, e.g. a structural frequency or a previous converged solution. Pre–computing the factors in the series (requiring $4n$ linear solves for the first order expansion), allows the application of the expansion in the vicinity of λ_0. Two approaches have been discussed. The quasi–Newton method evaluates the (exact) residual by solving one linear system of the form $(A_{ff} - \lambda I)\,\boldsymbol{y} = (A_{f\eta} + \lambda\, A_{f\dot{\eta}})\,\boldsymbol{p}_\eta$ and multiplying the solution $\boldsymbol{y}$ with the matrix A_{sf}, while the series approximation is used for the Jacobian matrix. The series method also applies the series expansion to the residual which is possible for small λ_ε and for an independent parameter μ not affecting the pre–computed values, thus excluding nonsymmetric aerostatic effects.

The main task in solving the small nonlinear eigenvalue problem in Eq. (2) is the evaluation of the Schur interaction matrix S^c as this involves computationally expensive operations on the high dimensional CFD–based fluid system. This matrix is influenced by the eigenvalue, particularly the frequency, and the steady state solution making it dependent on a large number of simulation parameters in the flow model, e.g. Mach number, angle of attack and dynamic pressure, and the structural model with the structural parameters defining the mode shapes. Hence, the evaluation of the matrix S^c will become prohibitively expensive to be applied in large scale aeroelastic stability analyses. For the evaluation of a computationally expensive function, such as the Schur interaction matrix, it is convenient to generate a cheap approximation based on relatively few runs of the expensive full order model. This surrogate is then used to provide information about the functional behaviour at untried parameter combinations. Several approaches to construct response surfaces can be found in the literature. In this study the Schur interaction matrix is reconstructed based on samples, i.e. full order evaluations of this term covering the parameter space of interest, using both the kriging interpolation technique and artificial neural networks as described in the following.

B. Extracting Samples of the Schur Interaction Matrix

The interaction matrix can be formed in both the frequency and time domain. Solving a number of n linear systems of the form $(A_{ff} - \lambda I)\,\boldsymbol{y} = (A_{f\eta} + \lambda\, A_{f\dot{\eta}})$ directly and multiplying the solution by the matrix A_{sf} to form the Schur interaction matrix is referred to as the linear frequency domain approach and is the preferred choice due to the computational cost involved in time domain simulations.

Alternatively in the time domain, the interaction matrix (i.e. the aerodynamic influence coefficient matrix) can be evaluated from the generalised forces $\boldsymbol{\Phi}^T \boldsymbol{f}$ following an excitation in the structural unknowns. One structural degree–of–freedom at a time can be excited in a forced sinusoidal motion at a fundamental frequency of $\lambda = i\,\omega$ applying a physically meaningful and mathematically consistent relation between deflection and deflection rate. The n generalised forces are Fourier–decomposed and divided by the corresponding Fourier coefficient of the forced structural motion. More elegant and efficient approaches to evaluate the

aerodynamic influence from unsteady CFD–based simulations over a range of frequencies can be used, such as an exponentially–shaped pulse excitation [29] or unit step/impulse excitation [7,30]. However, this is not needed in this study as powerful interpolation techniques are applied instead.

C. Approximating the Schur Interaction Matrix

Kriging Interpolation Technique

An excellent description on the background to the kriging approach was given in [31]. Herein only a brief overview is provided. In the kriging interpolation technique a multidimensional deterministic response of a simulation is treated as a realisation of a stochastic process. This process is composed of a low order regression model and a random normally distributed signal with zero mean and a covariance depending on the variance of the input samples and the correlation between two parameter locations. Thus, the second term (the error term) is not independent at different locations but is related to the distance between points in the parameter space. The parameters of the computationally cheap kriging model are determined for a known set of (typically expensive) numerical samples of the full order formulation by an optimisation process as given, for instance, in [31–33]. Importantly, the kriging predictor gives the exact system response at a sampled location with zero error in the kriging prediction.

Artificial Neural Network

A neural network is a collection of interconnected neurons or nodes with each node receiving a number of inputs either from the original input data, or from the output of other neurons in the network. The transfer of input to the node is weighted. Each node also has a single threshold value. The weighted sum of the inputs is formed, and the threshold subtracted, to compose the activation of the neuron. The activation signal is passed through an activation function to produce the output of the neuron.

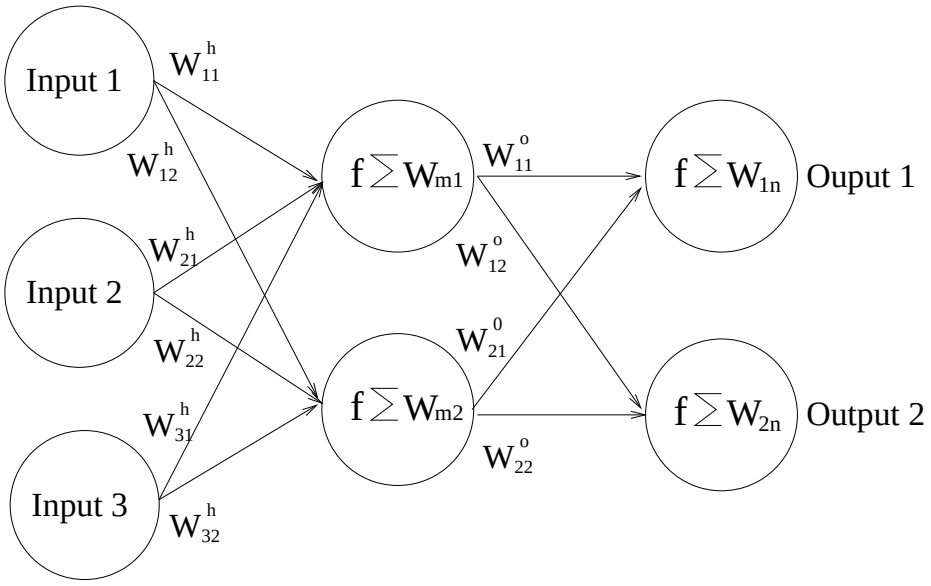

Figure 2. A typical ANN topology

Figure 2 shows a typical neural network with a layer of inputs, a hidden layer and an output layer. The input weights are summed and passed through an activation function, usually a nonlinear function like the hyperbolic tangent or exponential sigmoid. The output from the hidden layer forms the input to to the output layer. The weighted sum of the outputs from the hidden layer is once again passed through a linear

or nonlinear function to obtain the output. If the activation function in the hidden layers is nonlinear then the network has the capability to map the linear combination of system inputs to a nonlinear output. The most commonly used activation function is the sigmoid. The layers of nodes between the input and output are referred to as hidden layers and a network can have as many hidden layers as required. For smooth functions a few number of hidden units are needed, for fluctuation functions more hidden layers are usually necessary [34].

4. Application to Aeroelastic Stability Analysis

The interaction term depends on the frequency/damping and the parameters defining the steady state solution, including freestream Mach number, incidence, and the structural parameters influencing the structural mode shapes. Evaluating this matrix directly for each solution of the small nonlinear eigenvalue problem in Eq. (2) can become prohibitively expensive to be applied in routine calculations to search a larger parameter space for instability. The significant advantage of the approximation approach is that, once the interaction matrix can be represented by the surrogate model, the eigenvalue problem can be solved as often as necessary at very low computational cost. Then, any Newton–like method is a convenient choice to solve the nonlinear stability problem with the interaction term and its gradient readily available through the interpolation techniques, in this study using either kriging or artificial neural networks (ANN). The (wind–off) structural modes can be traced with changing values of the independent parameter and the critical eigenvalue with zero damping is detected using a bisection method.

In the current formulation the approximation of the interaction term is based on samples for a purely imaginary eigenvalue with zero damping, whereas the structural part uses the complete eigenvalue including a nonzero real part making it an analogy to the classical p–k method. In [19,20] it was shown that this is an appropriate simplification similar to the classical approach used for decades in production flutter analyses. Interestingly, for the flutter analysis using MSC.Nastran the aerodynamic influence coefficient matrix (which can be shown to be equivalent to the Schur interaction matrix) is evaluated at a limited number of points in the parameter space defined by the reduced frequency and freestream Mach number. This is necessary as this evaluation significantly contributes to the computational cost. An interpolation is applied to find the values between these discrete points [35]. Thus, the approach taken in this study is similar with two important differences. First, nonlinear CFD–based aerodynamic modelling is applied instead of the linear aerodynamic modelling used in MSC.Nastran. Secondly, the parameter space in the current approach can easily be extended to include more parameter dimensions.

In the following the general applicability of the approach in the transonic aeroelastic stability analysis is demonstrated using both kriging and ANN. Results are shown for an aerofoil case and two wing cases including the Goland wing and the multidisciplinary optimisation (MDO) wing.

A. Aerofoil Case

The approximate Schur complement matrix used for the stability analysis with the aerofoil structural model is written as

$$S = S^s(\lambda, \bar{u}) + \widehat{S}^c(\omega, M_r) \tag{5}$$

where $\widehat{S}^c$ is the approximation of S^c depending on the response frequency ω and the freestream Mach number M_r. For the considered aerofoil structural model, the correction term S^c is independent of the chosen bifurcation parameter, i.e. the reduced velocity $\bar{u}$, thus simplifying the discussion. At the critical eigenvalue $\lambda_F = i\,\omega_F$ the approximation is exact within the limits of the interpolation algorithm, while the introduced error away from the critical conditions was found to be small [19].

A representative element of the Schur interaction matrix in the frequency/Mach number parameter space for the Euler flow model is shown in Fig. 3 for the approximations based on both kriging and ANN. The upper limit of the freestream Mach number is defined by the buffeting boundary for the NACA 0012 aerofoil according to [36] while the (dimensionless) frequency range is chosen according to the structural frequencies as these indicate typical flutter frequencies. Note that the response frequency corresponds to the imaginary part of the eigenvalue. In the figure the real and imaginary parts of the response in the plunge degree–of–freedom due to changes in the plunge generalised coordinate are given for the NACA 0012 “heavy case”

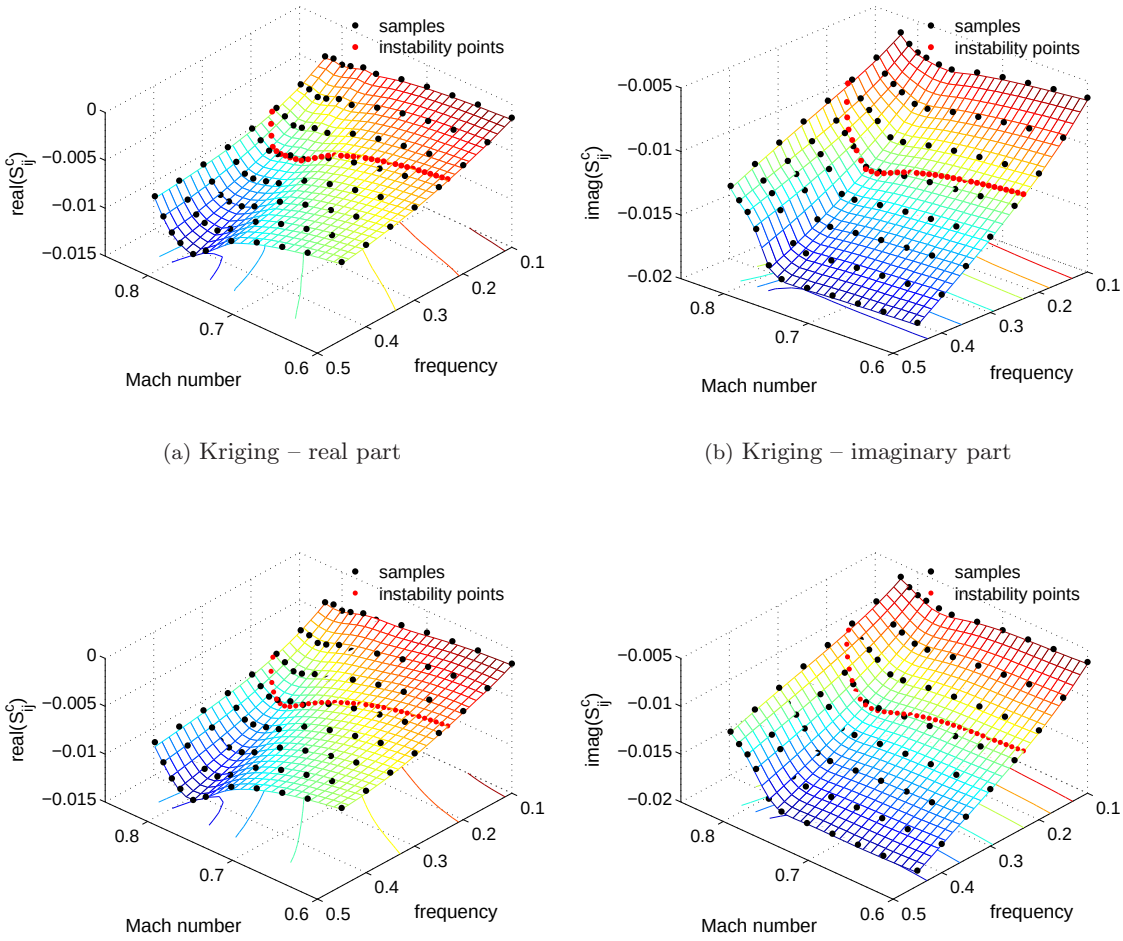

(a) Kriging – real part

(b) Kriging – imaginary part

(c) ANN – real part

(d) ANN – imaginary part

Figure 3. Extracted and interpolated element $S^c_{3,1}$ of Schur interaction matrix for NACA 0012 aerofoil configuration and Euler flow model including projected trace of instability; comparison of interpolations based on kriging and ANN.

aerofoil configuration, the structural parameters of which can be found in [14]. The black dots indicate sample locations, which were extracted using the linear frequency domain approach, while the colourful surfaces are the corresponding interpolations. The red dots describe the trace of the instability, projected onto the response surface, as critical values of the (dimensionless) response frequency with changing values of the freestream Mach number. The trace is included to illustrate the important regions of the parameter space. Recall that the steady state solution, and consequently the interaction matrix, can depend on a large number of system parameters. At this point of the current study for the demonstration using the simple aerofoil model problem only the dependence on the frequency and freestream Mach number is considered, while later on for the wing cases the input parameter space will be extended.

In Fig. 3 it can be seen that the two interpolation algorithms give indistinguishable response surfaces which should be expected considering the large number of true system evaluations. In the subsonic range the flow response (as expressed by the matrix elements) only has small changes with varying system parameters, while in the transonic range clear variations, in particular with respect to the freestream Mach number, are present. This behaviour is consistently found for all nonzero matrix elements and should be attributed to the formation of transonic shock waves.

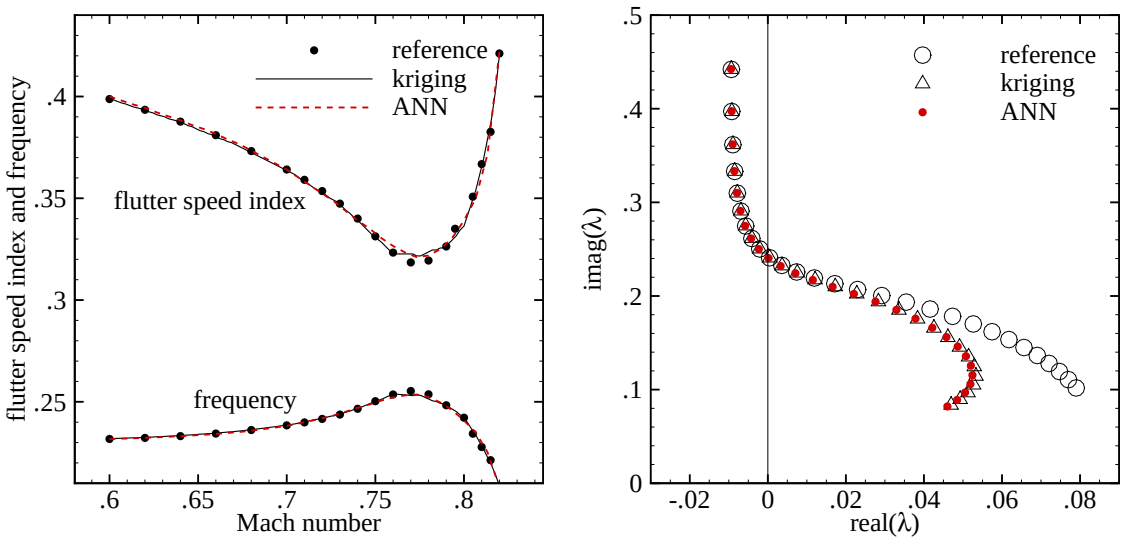

(a) Critical flutter speed index and frequency

(b) Mode tracing at Mach 0.8

Figure 4. Stability behaviour for NACA 0012 aerofoil configuration comparing interpolations based on kriging and ANN for Euler flow model and showing (a) critical values of flutter speed index and dimensionless frequency and (b) mode tracing of first (wind–off) structural mode at Mach 0.8.

Figure 4(a) presents the sub- and transonic instability boundary for the discussed NACA 0012 configuration. Critical values of the flutter speed index $V_F = \bar{u}/\sqrt{\mu_s}$ (where μ_s is the aerofoil–to–fluid mass ratio which is set to 100 for this configuration) and dimensionless frequency ω_F are shown. A comparison of results from the full order eigenvalue solver, defining the reference solution, and the approximation models is given and the agreement is excellent as expected considering the high sample resolution. The typical transonic dip for the bending/torsion type of instability is shown which is related to the formation of shock waves. A relation with the changes in the elements of the interaction matrix in the transonic range as found in Fig. 3 is evident.

The mode tracing of the least stable aeroelastic mode at Mach 0.8 with respect to changes in the reduced velocity is presented in Fig. 4(b) comparing the different approaches to the stability analysis. It can be seen that the trace is followed accurately even away from the imaginary axis. This suggests that the variation of the interaction elements with respect to the eigenvalue's real part (damping) is negligible and small compared with the structural contribution. The evaluation of 60 points on the root locus took less than a second of CPU time with each of the approximation models, whereas the exact Schur eigenvalue solver having a grid with 15 thousand control volumes took more than one hour (about one minute per point) on a modern desktop personal computer using the quasi–Newton method. On the other hand, unsteady time marching at an individual reduced velocity using a dimensionless time step of 0.05 for temporal accuracy takes more than 10 minutes per cycle of motion (comprising about 500 steps) while typically five to ten cycles are required to establish a periodic oscillatory motion with negligible nonperiodic transients due to the initial disturbance of the steady state.

B. Wing Cases

For wing cases the Schur complement matrix S in Eq. (3) is conveniently written as

$$S = \left(C_1 + \mu\, C_2 - \lambda I\right) - \mu\, C_3\, (A_{ff} - \lambda I)^{-1}\, (A_{f\eta} + \lambda\, A_{f\dot{\eta}}) \tag{6}$$

where the matrices C_1, C_2 and C_3 follow directly from the equations of the matrices A_{ss} and A_{sf} given in the previous section describing the modal structural model. This form allows the evaluation of the matrices C_2

and C_3 independently from the bifurcation parameter μ, typically representing the dynamic pressure. The approximated Schur complement matrix used for the stability analysis, including the parameter dependencies, is then written as

$$S = S^s(\lambda, h_r, M_r) + \mu(h_r, M_r)\,\widehat{S}^c(\omega, h_r, M_r) \tag{7}$$

where h_r indicates the dependence on the altitude in addition to the freestream Mach number as matched simulations are generally discussed. Additional parameters defining the steady state solution, such as the angle of attack, can be included in this notation. A matched simulation is done by varying the altitude and adjusting the values of the density and speed of sound according to the standard atmosphere conditions. Then, the velocity follows from the current freestream Mach number. The matrix $S^s = C_1 + \mu\, C_2 - \lambda I$ is the structural part where the term $\mu\, C_2$ is often (but not generally) negligible as it is orders of magnitude smaller than the other terms [20]. The expression $\widehat{S}^c$ is the interpolation approximation of the modified interaction term $\widetilde{S}^c = -C_3\,(A_{ff} - \lambda I)^{-1}\,(A_{f\eta} + \lambda\, A_{f\dot{\eta}})$ excluding the bifurcation parameter. The roots of the approximated Schur residual are found by any Newton–like method. As for the aerofoil case, the interaction term is sampled for eigenvalues with zero damping while the structural part uses the complete eigenvalue. This simplification is appropriate as will be seen in the following discussion.

Symmetric Goland Wing/Store Configuration

First, the symmetric case without aerostatic deflection is discussed which makes the modified interaction term $\widetilde{S}^c$ independent of the altitude as the matrices A_{ff} and $A_{fs} = [A_{f\eta}, A_{f\dot{\eta}}]$ only contain sensitivities of the fluid system which is, by default, made dimensionless by freestream reference values. Using the notation in Eq. 6, the construction of the approximation model without aerostatic effects is simplified in the sense that a matched simulation only requires the adjustment of the independent parameter to the current value of the reference density while the other part $\widetilde{S}^c$ of the computationally expensive interaction term S^c is sampled for different values of the response frequency and freestream Mach number. The matrix $C_1 = D$ also needs to be matched to the current reference values as the normal mode frequencies are made dimensionless using the reference freestream velocity. This is a trivial task. The matrix C_2, containing the sensitivity of the force vector with respect to the deformation at fixed flow solution, is neglected in the first instance as it was found to be several (typically 3 to 5) orders of magnitude smaller than the other terms.

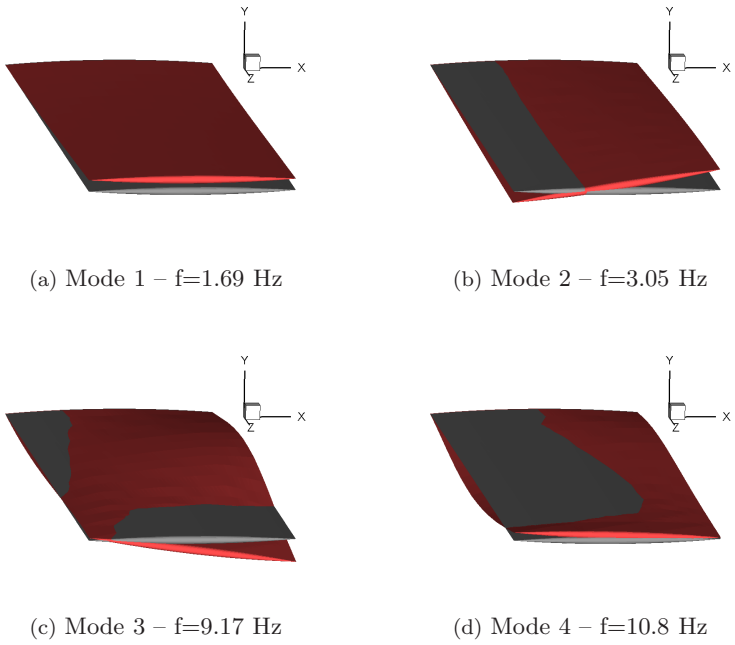

(a) Mode 1 – f=1.69 Hz

(b) Mode 2 – f=3.05 Hz

(c) Mode 3 – f=9.17 Hz

(d) Mode 4 – f=10.8 Hz

Figure 5. Mode shapes of Goland wing/store configuration.

The Goland wing, as such a symmetric case, is a model wing having a chord of 1.8266 m and a span of 6.096 m. It is rectangular and cantilevered with a constant cross section defined by a 4% thick parabolic–arc aerofoil. The finite–element model, used to calculate the mode shapes for the modal structural model in the CFD formulation, follows the description given in [37]. The wing/store case is discussed retaining the four modes with the lowest frequencies (excluding in–plane modes) for the aeroelastic simulations. The frequencies as well as the mode shapes mapped to the CFD surface mesh are shown in Fig. 5. Here, a relatively large value of two is chosen for the modal amplitudes for illustration purposes. A computational mesh with 200 thousand control volumes is used for the current Euler simulations while the store aerodynamics are not modelled.

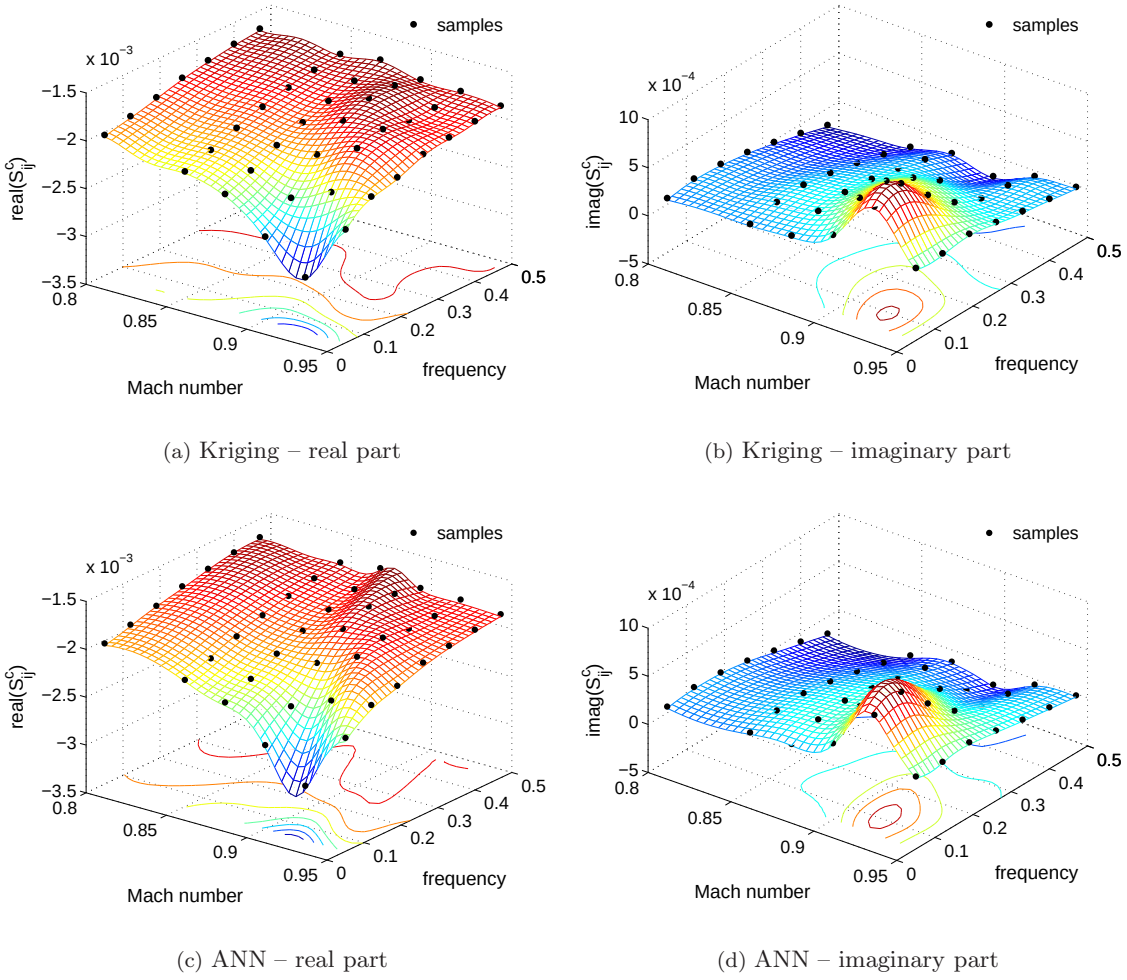

(a) Kriging – real part

(b) Kriging – imaginary part

(c) ANN – real part

(d) ANN – imaginary part

Figure 6. Extracted and interpolated element $S^c_{5,2}$ of Schur interaction matrix for Goland wing/store configuration and Euler flow model; comparison of interpolations based on kriging and ANN.

In the common situation, the structural grid points $\boldsymbol{x}_s$ not only do not conform with the aerodynamic surface grid, but are also defined on different surfaces. This requires the transfer of information between the fluid and structural grids. The aerodynamic (pressure) forces, defined at the CFD surface grid, have to be transferred to the structural grid, and the modal deflections $\delta\boldsymbol{x}_s$ have to be communicated back to the CFD surface mesh. This is achieved in the current formulation using a method called the constant volume tetrahedron (CVT) transformation [38] which is a local intergrid transfer method. Thus, the grid locations at the boundaries of structural elements (defined by three structural grid points) are matched while the slope is not, and it was found that this intergrid transformation performs badly when required to extrapolate [20,39].

Such an extrapolation to the trailing edge line is required behind the two thirds chord line of the Goland wing resulting in a zigzag–like mapping of the trailing edge region. To improve the situation and to eliminate a possible pollution of the results, the original mode shapes are re–defined to avoid extrapolation using CVT. The mode shapes are linearly extrapolated to the trailing edge line at each spanwise location (rib) of the finite–element model as a preprocessing step before they are applied in the intergrid transfer formulation in the CFD solver.

Figure 6 gives one representative element of the (modified) Schur interaction matrix for the wing/store configuration showing real and imaginary parts individually. The reconstruction of the response in the first degree–of–freedom with respect to changes in the second generalised coordinate is presented using both kriging and ANN interpolation. The reconstruction is based on 42 samples covering a Mach number range between 0.8 and 0.95 and a dimensionless frequency range between 0.05 and 0.45. For a defined number n of considered normal modes, a $2n \times 2n$ Schur complement matrix is formed with n^2 nonzero complex–valued elements corresponding to an output dimension of $2n^2$ for the interpolation models. The differences between the two interpolation techniques is small and the response surface shows a similar behaviour as for the aerofoil case. In the subsonic region, only small changes can be found with respect to the input dimensions of frequency and freestream Mach number, while there are significant variations in the transonic range.

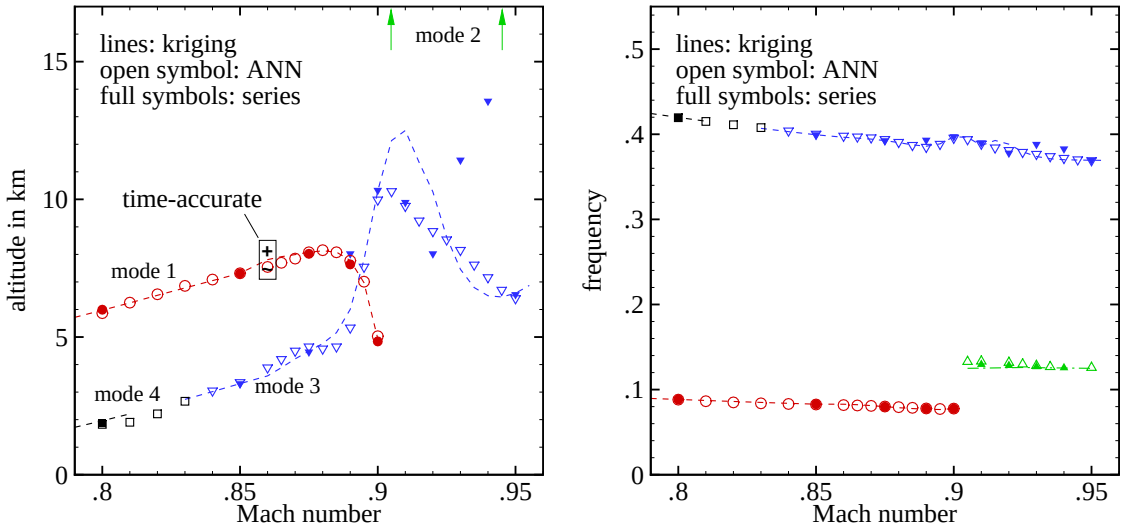

(a) Critical altitude

(b) Critical frequency

Figure 7. Stability behaviour for Goland wing/store configuration comparing interpolations based on kriging and ANN for Euler flow model and showing critical values of altitude and dimensionless frequency including instability points for all modes.

The more distinct changes in the response surfaces above a freestream Mach number of 0.9 are related to the formation of shock waves and result in significant changes in the instability boundary, leading to shock induced limit–cycle oscillation (LCO) for this wing/store case [37]. The instability boundary for the configuration is presented in Fig. 7 showing critical values of the altitude and dimensionless response frequency for all four modes originating in the wind–off structural modes. Importantly, the approximation approaches using both kriging and ANN give excellent agreement with the full order predictions based on the series method. Between freestream Mach numbers of 0.905 and 0.945 the aeroelastic system is unstable right from the start of the considered altitude range at 30 km. The instability is dominated by the second mode which is a torsion mode. In this range for the second mode instability the differences in the third mode instability as obtained from the three prediction methods are not of immediate interest for the linear stability analysis and are not discussed in more detail. The time–accurate results included in the figure match the eigenvalue–based predictions precisely.

Figure 8 shows the tracing of the four wind–off structural modes with respect to altitude changes at a freestream Mach number of 0.875 and compares the full order predictions with results from the approximation models using both kriging and ANN. The interpolation models are based on the samples shown in Fig. 6. The full order predictions were obtained by applying the series method with a second order expansion. The agreement in both the mode tracing and the onset of the instability is excellent. The results show a classical binary instability mechanism with an instability occurring alongside the interaction of two aeroelastic modes involving the first bending and first torsion mode. In addition, the wing/store case gives a second instability at lower altitudes following the interaction of the third and fourth mode.

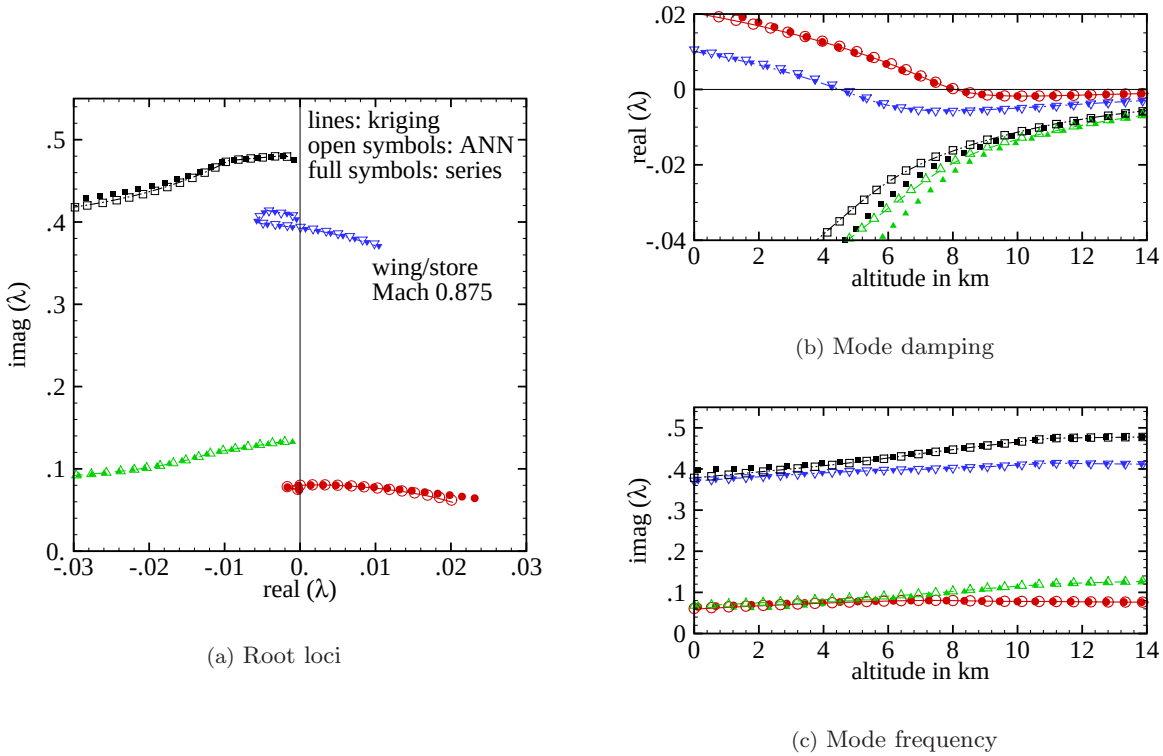

(a) Root loci

(b) Mode damping

(c) Mode frequency

Figure 8. Mode tracing at Mach 0.875 with respect to altitude for Goland wing/store configuration comparing full order series results with approximation results using kriging and ANN; eigenvalues given in dimensionless form.

For the reconstruction of the response surface in Fig. 6, a number of 42 samples is used corresponding to the cost of $42 \times n$ linear solves against the high dimensional fluid system once the steady state solution is available. In the following one linear solve is taken as an equivalent cost factor because the solutions of the large sparse linear systems incur most of the involved computational cost. These samples allow the stability analysis covering an entire range of freestream Mach numbers between 0.8 and 0.95. Using the series method with a first order expansion only, the evaluation of the series factors for all n normal modes takes $n \times 4n$ linear solves per steady state solution, i.e. per freestream Mach number in this example, while tracing the modes can then be done essentially without additional cost with available series factors. Thus, the cost invested in constructing the approximation models pays off with a full order stability analysis at the third freestream Mach number. Also, the reconstruction approach becomes more powerful with an increasing number of normal modes as every individual sample supports the analysis/tracing of all modes while the series factors are only valid close to the shift, e.g. the normal mode frequency, they have been evaluated for. Once the approximation model is established, the stability analysis can be done essentially without additional cost no matter how large the original CFD–based system becomes. The aim of using either kriging or ANN to

interpolate the elements of the interaction matrix is to reduce the number of calculations for a blind search stability analysis over the flight envelope, i.e. for a range of flow conditions. However, for a single point analysis excluding the effects of aerostatic deformation it seems to be more efficient to use the series method as the surrogate models require a minimum number of samples.

Nonsymmetric MDO Wing Configuration

Secondly, the nonsymmetric case including the effects of aerostatic deflection is discussed. The general influence of the aerostatic deformation on the transonic steady state solution with varying altitude is that a decreasing altitude, corresponding to an increase in the dynamic pressure, causes the wing to bend up and to twist the nose down slightly at the wing tip, resulting in a weakened shock wave. The modified interaction term $\widetilde{S}^c$ in Eq. 7 becomes dependent on the altitude. As a consequence, the sampling has to cover the altitude range of interest. This however is equivalent to the requirements of the exact (full order) eigenvalue solver. Using the series method, the factors have to be re–evaluated constantly as the modes are traced with changing altitude. Here, the altitude change before re–evaluating the series factors depends on the demanded accuracy. As will be seen below, the approximation of the (modified) interaction term using the interpolation approaches becomes very attractive concerning the cost.

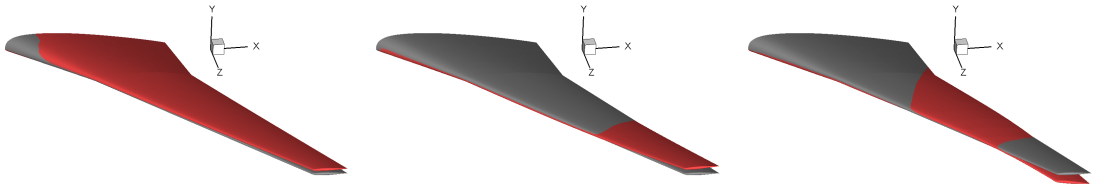

(a) Mode 1 – f=0.84 Hz (b) Mode 2 – f=2.16 Hz (c) Mode 3 – f=3.56 Hz

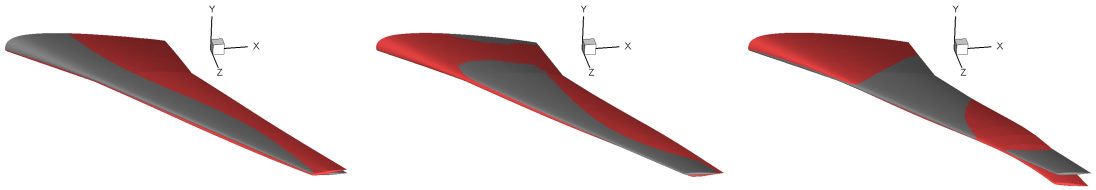

(d) Mode 4 – f=3.99 Hz (e) Mode 5 – f=5.01 Hz (f) Mode 6 – f=5.37 Hz

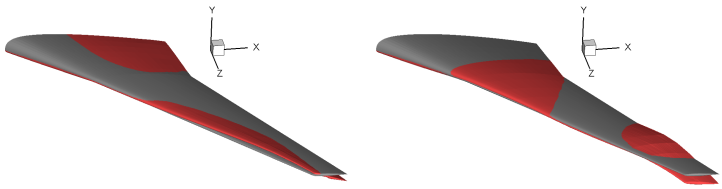

(g) Mode 7 – f=6.57 Hz (h) Mode 8 – f=7.30 Hz

Figure 9. Mode shapes of MDO wing configuration.

The multidisciplinary optimisation (MDO) wing is a highly flexible, commercial transport wing designed to operate in the transonic range. It has a span of 36 m and a thick supercritical section. The nonsymmetric section makes the steady state solution dependent on the altitude as the nonzero force vector in the governing

structural equations has to be balanced by the stiffness terms. The finite–element model is given by a wing box along the central portion of the wing [17]. For the aeroelastic stability analysis a total number of eight normal modes is considered with the mode shapes, mapped to the CFD surface grid, and the normal mode frequencies given in Fig. 9. A computational mesh with 65 thousand control volumes is used for the discussed Euler simulations. This case is chosen to demonstrate the applicability of the presented approximation approaches both to a higher number of normal modes and to an expanded space of independent parameters. Due to the virtual design of the MDO wing, experimental data are not available.

The challenge for the interpolation techniques as discussed up to this point is not the inclusion of aerostatic effects at fixed freestream Mach number but the search for aeroelastic instability over the flight envelope, i.e. a range of freestream Mach numbers. Therefore, a three dimensional parameter space including the response frequency, altitude and freestream Mach number is considered in Fig. 10. The distribution of 252 samples for the reconstruction of the interaction matrix is shown including the trace of the first and second mode instabilities with changing values of the freestream Mach number to illustrate the important part of the parameter space. The samples were distributed using uniform grid sampling covering the parameter space of interest (concerning the altitude and Mach number) and relevance (concerning the dimensionless response frequency which follows the structural frequencies). The contour slice for one representative element of the interaction matrix at the freestream Mach number of 0.80 is included. The differences in the contour slices obtained from the two interpolation approaches are rather small as are the stability results which are discussed in the following.

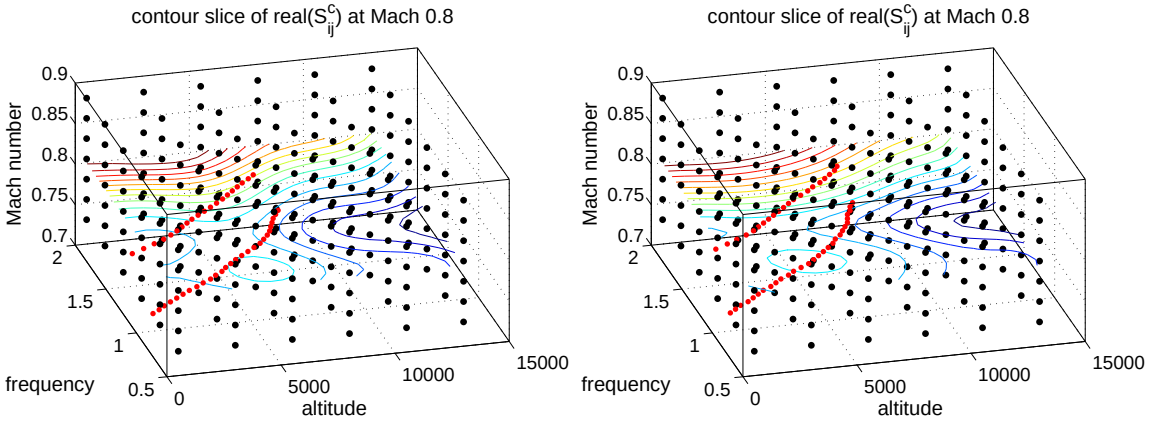

(a) Kriging

(b) ANN

Figure 10. Three dimensional grid sampling for MDO wing configuration and Euler flow model showing approximated element real($S^c_{10,1}$) of Schur interaction matrix including instability points; interpolations based on kriging and ANN.

The stability limit of the MDO wing configuration over a range of freestream Mach numbers between 0.7 and 0.9 is presented in Fig. 11 as critical values of altitude and dimensionless response frequency. The effects of the aerostatic deformation are fully accounted for. The results of the approximation approaches are compared with full order evaluations, and an accurate agreement between the kriging, ANN and full order results is found. For freestream Mach numbers below 0.75, the configuration only encounters aeroelastic instability below sea level while at common cruise conditions the critical region starts at about 5 km. The first mode instability is the critical mode in most parts of the considered Mach number range. In addition, the first mode exhibits a second bifurcation at the highest Mach numbers which is below the second mode instability, and therefore not of immediate interest. This second bifurcation is not found with the approximation approaches for the chosen sample distribution. Time–accurate results at one freestream Mach number, herein only shown for the response frequency but not the altitude, match the eigenvalue–based results precisely.

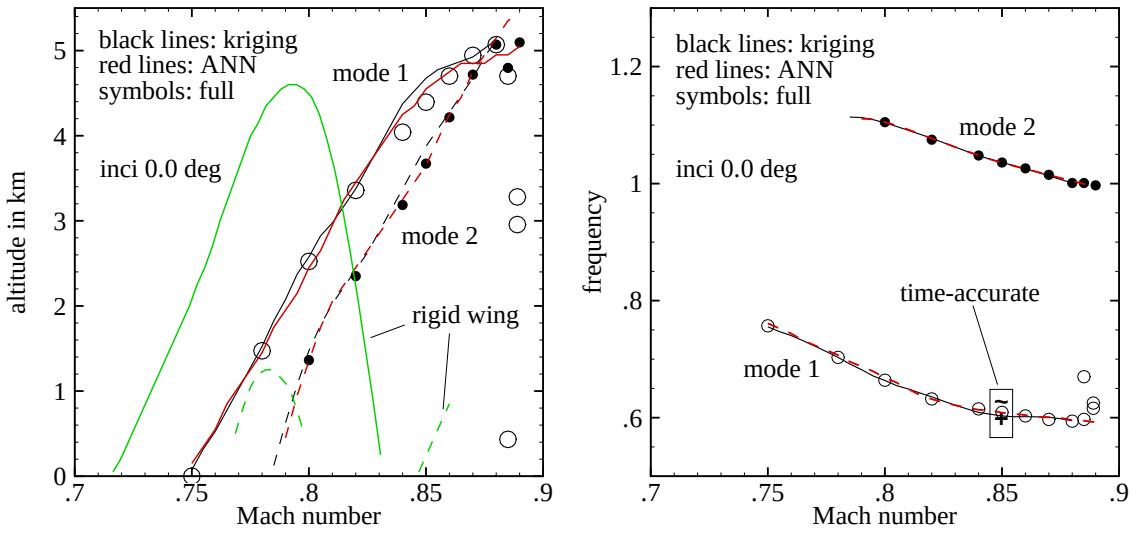

(a) Critical altitude

(b) Critical frequency

Figure 11. Stability behaviour for MDO wing configuration comparing interpolations based on kriging and ANN for Euler flow model and showing critical values of altitude and dimensionless frequency

The influence of the small second term μC_2 in the structural part of Eq. (6) was considered for the kriging approach for the sake of completeness. Therefore, a second kriging model was formed based on full order samples which are routinely evaluated alongside the samples of the interaction term. These samples allow the reconstruction of the corresponding response surfaces depending on the altitude and freestream Mach number. These "improved" predictions are within plotting accuracy compared with the results given in Fig. 11 reflecting the dominance of the stiffness and interaction terms in this example. These results are neither shown nor further discussed.

The number of 252 samples used to represent the physics in the parameter space for the reconstruction of the interaction matrix seems to be large. This is discussed now. Using the full order series method, assume that four Mach numbers along a flight envelope are to be investigated while accounting for aerostatic effects. For an altitude search range of 15 km, re–evaluating the series factors (for a first order series expansion) only four times creates an equivalent cost of $4 \times 4 \times n \times 4n$ linear solves for the eight normal modes. The chosen decrement in altitude of about 4 km before re–evaluation clearly introduces uncertainty and inaccuracy in the predictions. Thus, the 252 samples, requiring $252 \times n$ linear solves, generate about half the cost compared with the series method while giving accurate results. Note, for the current results the series factors were calculated at each new altitude (which makes it quasi–Newton) for reasons of accuracy when comparing with the approximation models.

Importantly, in Fig. 11(a) an additional set of results, labelled "rigid wing" and taken from [20], is shown to illustrate the importance of considering the effects of aerostatic deformation in transonic aeroelastic stability analysis. For the rigid wing results, the geometry is not allowed to deform for the steady state solution which strictly does not balance the nonzero force vector with the stiffness terms resulting in a nonzero structural residual $\boldsymbol{R}_s$. It can be seen that the first mode instability forms the typical transonic dip shifted to lower freestream Mach numbers which can be explained by recalling the effect of the aerostatic deformation on the steady state solution. The aerostatic deformation causes the wing to bend up and to twist the nose down slightly at the wing tip. This results in a weakened shock wave compared with the aerostatically rigid wing. In the figure it can be seen that aerostatic deformation cannot be ignored.

The tracing of the eight wind–off structural modes with changing values of the altitude at a freestream Mach number of 0.8 is presented in Fig. 12. Compared with the full order results using the series method, the figure shows an accurate tracing of all considered modes using both the kriging and ANN approximation

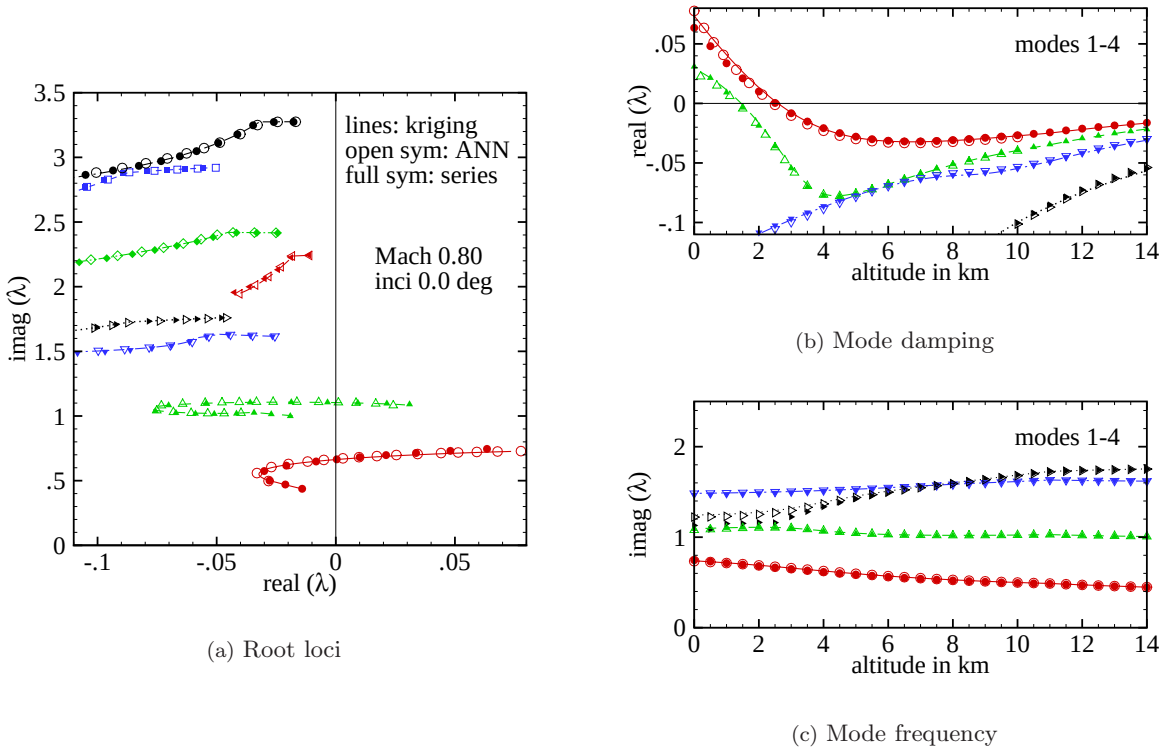

(a) Root loci

(b) Mode damping

(c) Mode frequency

Figure 12. Mode tracing at Mach 0.8 with respect to altitude for MDO wing configuration comparing full order series with approximation results using kriging and ANN; eigenvalues given in dimensionless form.

of the interaction matrix elements. Here, the series factors (just as the steady states) were re–evaluated at each new altitude for reasons of accuracy for the comparisons with an applied decrement of 500 m. The first mode goes unstable at an altitude of about 2.5 km, closely followed by the second mode crossing the imaginary axis at about 1.5 km. The differences in the frequency at lower altitudes for the fourth mode are due to the strongly damped character of this mode. The assumption of a simple harmonic aerodynamic response, i.e. $S^c(\omega)$ instead of $S^c(\lambda)$, does not hold in this case. However, this behaviour is irrelevant for the stability prediction.

C. Summary for General Applicability

The task in this preceding section was to demonstrate the applicability of approximating the computationally expensive Schur interaction matrix, representing the aerodynamic influence on the modified structural eigenvalue problem, in transonic aeroelastic stability analyses. The results from the approximations based on kriging and ANN were compared with those from the full order eigenvalue solver. Three test cases were discussed including a NACA 0012 aerofoil configuration and the Goland and MDO wing cases. Importantly, both interpolation techniques give excellent agreement with the full order results, and neither approximation approach seems to be superior to the other. This observation is not too surprising considering the densely sampled parameter spaces used so far in this paper. Most likely, any robust interpolation algorithm would allow a similar conclusion.

The stability calculations using the approximation models are very cheap. However, the approximation models require true (expensive) samples for the Schur interaction matrix from the exact eigenvalue solver while covering the parameter space of interest to represent the important physics. Up to this point the large number of samples, corresponding to a relatively high cost, are distributed over the parameter space using a very basic, brute force, rectangular grid sampling approach. In the next section more efficient sampling techniques, which are tailored for the purpose of this study to search parameter spaces for instability, will

be presented making the approach of sampling and reconstruction for the stability analysis very attractive in terms of cost. It is important to remark that, despite the large number of samples used for the test cases shown above, the approximation models have already been demonstrated to be computationally more efficient than the full order approach when applied over a larger parameter space.

5. Instability Searches Using Coordinated Sampling

The cost to create an approximation model, i.e. the required number of samples to adequately represent the variation in the elements of the interaction matrix within the parameter space, is an important factor in the aeroelastic stability analysis especially for an expensive high fidelity aerodynamic model. It is a standard practice to replace a computationally expensive multidimensional model by an inexpensive surrogate using, for instance, artificial neural networks or kriging tools. This is the topic of the current paper. Then, the two main tasks of the analysis are to distribute a few true evaluations of the expensive function over the parameter space in order to allow an accurate representation of the important physics, and to use the surrogate to reconstruct/approximate the functional behaviour efficiently, robustly and precisely. The important task of sampling is analysed in the following.

Space–filling algorithms, such as grid sampling used in the preceding section, tend to require an excessive number of samples to achieve the demanded accuracy. Studying the eigenvalue–based aeroelastic stability analysis, it was found that it is neither necessary to accurately approximate the response surfaces of the interaction matrix components globally, nor useful to apply an optimisation algorithm to locate a global extremum in the interaction matrix components. Here, the expression "global" refers to covering the entire parameter space within its bounds. A globally accurate approximation of the interaction matrix is not required for the linear stability problem as the interest focusses on detecting the most critical conditions. Particularly, analysing both the structural governing equations and the modified structural eigenvalue problem of the Schur method, it is clear that the influence of the computationally expensive interaction term on the eigenvalue problem can be quite different. Low values of the dynamic pressure (represented in this study by either the reduced velocity or the altitude) cause the influence of the fluid interaction to be low. As a consequence an inaccurate approximation of the interaction matrix can still give precise results. High dynamic pressures, on the other hand, result in a strong fluid/structure interaction demanding a better approximation. Also, individual aeroelastic modes can be rather insensitive to the fluid response. A global optimisation, on the other hand, is not useful because an extremum in the Schur interaction matrix elements not only does not necessarily correspond to the point of instability but also the functional extrema of the interaction term are commonly outside the relevant region (and outside the specified parameter bounds) as can be seen in the example results given in the previous section.

Thus, the sample distribution should be tailored to the aeroelastic problem. The approach chosen, introduced in [19] as risk–based sampling, exploits the approximation models to focus new sample locations in the vicinity of the converged instability boundary. Here, starting from the corner points of the parameter space giving 2^m initial samples (with m as the number of independent parameter dimensions), an approximation model is always formed for the current set of samples which is then used to run the complete instability search. This is possible because of the low computational cost using the approximation model. A new sample is selected along the current approximation to the converged instability boundary, and this selection process is distinct for the two interpolation techniques discussed. As will be seen in the following, the sampling approach converges rapidly to satisfy predefined stopping criteria.

A. Aerofoil Case

As a first example, the above NACA 0012 "heavy case" aerofoil configuration is analysed. The Euler equations are applied using a computational mesh with 15 thousand control volumes. The initial search region is defined in the frequency/Mach number parameter space limiting the frequency range for the structural frequencies and the sub- and transonic Mach number range according to interest. As mentioned before, starting from the current set of samples the approximation models (kriging and ANN) are formed/trained and used to perform complete stability analyses giving an approximation to the converged instability boundary as critical values of the reduced velocity and response frequency. The selection of a new sample location is different for kriging and ANN.

A measure of error for the kriging prediction is readily available as integral part of the kriging formulation as it is based on a stochastic process model [31]. This is a very convenient characteristic of the kriging approach giving the prediction of the interaction matrix elements together with a measure of the confidence in this prediction. Naturally, a new sample is placed along the current evaluation of the instability boundary where the kriging error is highest. This approach allows the placement of samples where it is needed most to support the stability analysis, i.e. close to the instability, and to improve the kriging approximation, i.e. at the point of highest error.

Such an analysis is presented in Fig. 13. The distribution of samples in the paramater space demonstrates how the samples gather around the converged instability boundary. As the kriging error depends on the distance between samples, the samples are uniformly distributed making the risk–based sampling a constrained space–filling algorithm, constrained in the sense that a new sample location requires a previous instability point. The approach converges rapidly as can be seen in the figure. With the sixth iteration starting from the four initial corner samples, the instability boundary is accurately predicted compared with the full order reference solution. Importantly, once the iteration results in placing samples close to each other as the instability boundary is accurately detected, the iteration must stop to avoid a numerically unstable kriging model which follows from the ill–conditioning of the kriging correlation matrix. Two closely located samples correspond to two columns in the correlation matrix to be nearly identical giving a nearly singular matrix [31].

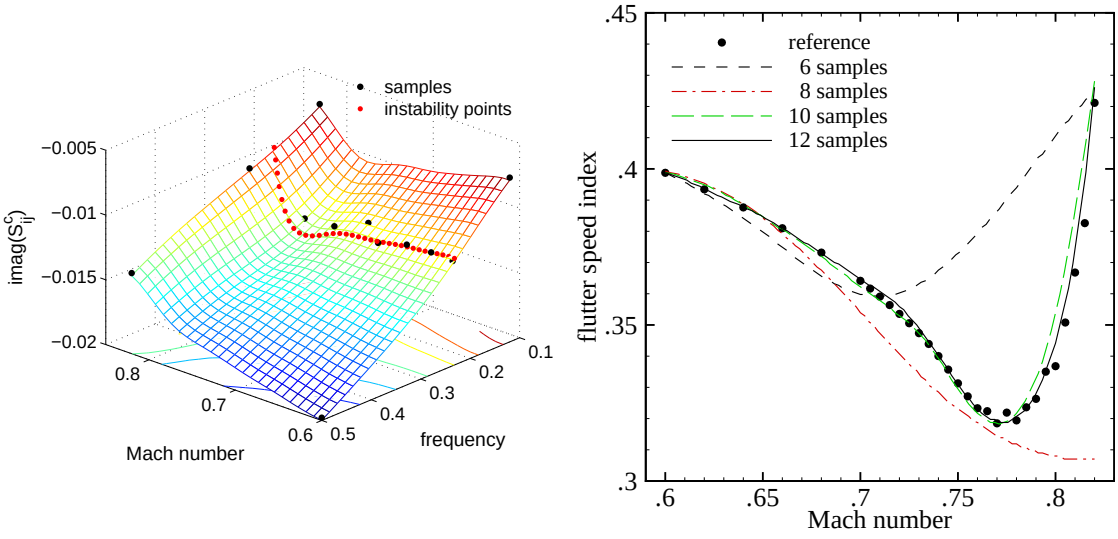

(a) Element imag($S^c_{3,1}$) based on 12 samples

(b) Critical flutter speed index

Figure 13. Risk–based sampling for NACA 0012 aerofoil configuration using kriging interpolation and showing (a) representative element of Schur interaction matrix including projected trace of instability and (b) critical flutter speed index compared to reference solution.

As a measure of error is not readily available for the current ANN formulation, a different approach has been chosen instead to search for aeroelastic instability. Starting from the stability results obtained from the analysis using the ANN model trained for the initial four corner samples, the first iterative sample is placed randomly along the current approximation to the converged instability boundary. Following this startup, new samples are always placed along the current instability boundary at the location where the difference to the prediction at the previous iteration step is highest. This difference can also be used as one possible convergence criterion. As shown in Fig. 14, this approach results in the samples being clustered in the important regions similar to the kriging risk–based sampling discussed above. The convergence of the instability boundary proceeds in a similar fashion giving an accurate prediction compared with the reference solution in about ten samples.

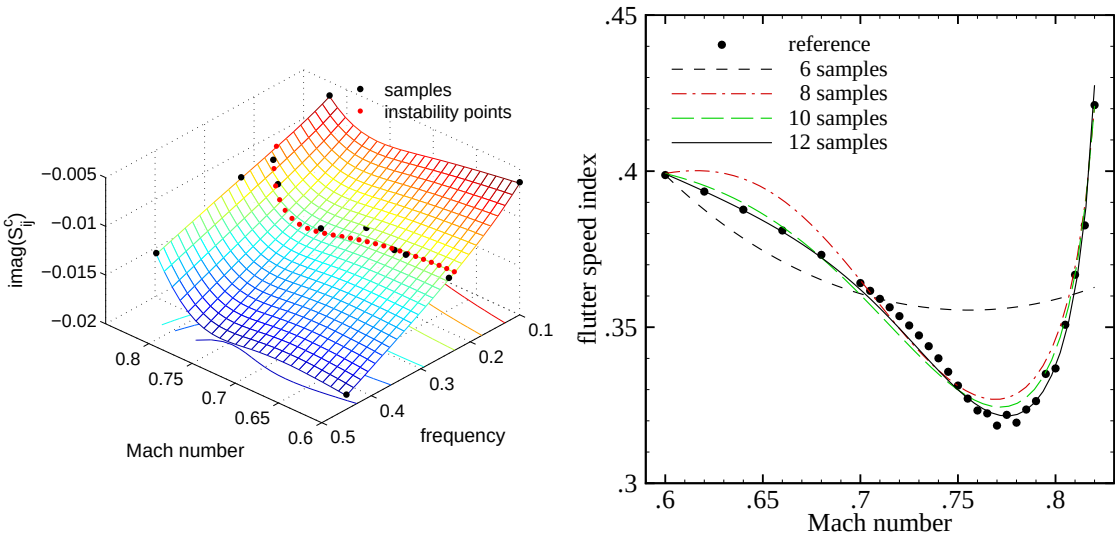

(a) Element imag($S^c_{3,1}$) based on 12 samples

(b) Critical flutter speed index

Figure 14. Risk–based sampling for NACA 0012 aerofoil configuration using ANN interpolation and showing (a) representative element of Schur interaction matrix including projected trace of instability and (b) critical flutter speed index compared to reference solution.

Evaluating the entire response surface for the interaction matrix elements precisely within the initial search space is not attempted with the risk–based sampling approach. As a consequence, the mode tracing could become inaccurate further away from the instability which, however, would be a fair trade–off compared with the cost. If this inaccuracy becomes critical, i.e. resulting in an eigenvalue with a positive real part, then the sampling criterion would automatically place a new sample in this region to correct the prediction. This is not the case for the NACA 0012 aerofoil problem discussed herein. Looking at Fig. 15, it can be said that the root locus of the critical mode is reproduced well using the twelve risk–based samples for both kriging and ANN. In the most important region close to the imaginary axis the agreement with the results of the exact eigenvalue solver, referred to as "reference" and shown in Fig. 4(b), is accurate. This can be explained by interpreting the governing equations for the aerofoil structural model given in Section 2. The reduced velocity $\bar{u}$, as the independent parameter, enters the eigenvalue problem by its square in the denominator of the stiffness matrix. Thus, for small values of $\bar{u}$ the influence of the structural part S^s on the eigenvalue problem is higher, while with increasing values of $\bar{u}$ the influence is reduced making the fluid interaction more important. The approximation of the interaction matrix is good enough in regions where the structural part dominates the problem. However, once the interaction term becomes more active closer to the instability, the parameter space is sufficiently covered by samples. For values of the reduced velocity well beyond the instability onset,

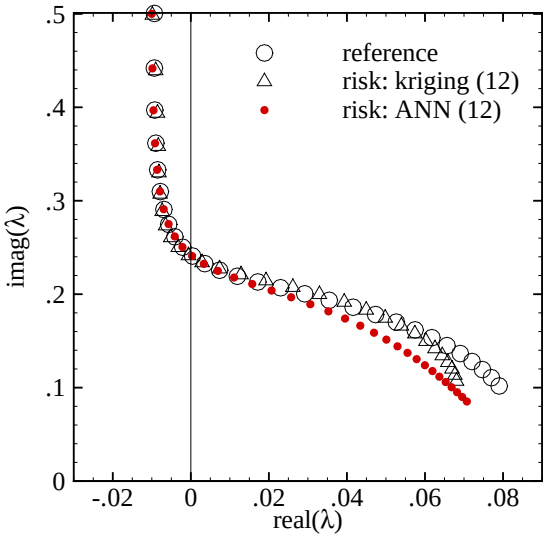

Figure 15. Mode tracing for risk–based sampling using twelve samples for kriging and ANN at Mach 0.8.

the agreement between the different approaches is less accurate for two reasons. First, the parameter space is undersampled to represent the stong fluid/structure interaction. Secondly, the simplification of using exact numerical samples for zero damping, i.e. $S^c(\omega)$ instead of $S^c(\lambda)$, naturally loses accuracy. This latter point was already observed in Fig. 4(b) for the dense uniform grid sampling.

Having the steady state solutions, the cost to extract the ten samples, sufficient in this example to cover a complete sub- and transonic regime, corresponds to the cost of $10 \times n$ linear solves against the fluid system. On the other hand, the cost to form the factors in the series expansion in Eq. (4) for the two normal modes of the aerofoil case at one individual freestream Mach number requires $n \times 4n$ linear solves. Thus, with the second Mach number the construction of the approximation models pays off. To compare with time domain predictions, the simulation of one cycle of motion at one combination of freestream Mach number and reduced velocity corresponds to about ten to 20 steady state solves using a dimensionless time step of 0.05 for temporal accuracy (where one steady state solution corresponds to about $2n$ linear solves in this example). Typically four to five values of the reduced velocity are required per Mach number to bracket the instability, and more than one cycle of motion is required to identify the system response following an initial disturbance. Thus, the stability analysis at only five Mach numbers, to trace out the instability boundary, is at least two orders of magnitude more expensive than the eigenvalue–based approach using the approximation models.

B. Wing Cases

The risk–based sampling approach for the wing configurations to search larger parameter spaces efficiently for aeroelastic instability proceeds in a fashion similar to the aerofoil case. First, an initial search space is defined by the corner samples with the frequency range chosen according to the structural frequencies and any additional parameter dependencies chosen according to the region of interest. Then, the wind–off structural modes are traced with varying altitude under matched conditions using the cheap approximation models always based on the current set of samples, and the instability points are detected in the parameter space. Alternative sampling criteria, for example a positive gradient in the eigenvalue's real part with respect to the altitude, are possible. As for the aerofoil case, the selection of a new sample location is distinct for the two approximation approaches due to the distinct characteristics of the tools. The selection criteria follow the aerofoil formulation. Using kriging interpolation, the detected instability point corresponding to the highest error in the prediction of the interaction matrix gives a new sample location. Using ANN interpolation, the maximum change in successive instability boundaries defines the new sample location with the sample being placed according to the most recent instability prediction.

For realistic configurations, multiple instability points can often be found as was presented for both the Goland wing/store and MDO wing configurations. However, only the most critical condition, i.e. the highest altitude encountering the instability, is then considered in the current paper as any additional instabilities within the unstable region are not of immediate interest for the linear aeroelastic stability analysis.

Goland Wing/Store Configuration

In Figs. 16 and 17 the risk–based sampling to search for instability is presented for the Goland wing/store configuration. The reference solutions are taken from the previous section. Figure 16 gives the convergence of the instability boundary with increasing numbers of samples for both kriging and ANN. The convergence behaviour for the two interpolation models is similar. After about 20 samples the instability boundary giving the most critical altitude is accurately predicted. Note that the bucket of limit–cycle oscillation between Mach 0.905 and 0.945 defined by the second mode instability is only detected towards the end of the iterations. Here, the samples are placed initially according to either the first or third mode instabilities not allowing an appropriate representation of the interaction matrix to detect the second mode instability. However, even for this rather complicated behaviour the risk–based sampling approach converges.

The distribution of 20 samples together with the approximation of the response surface of a representative matrix element and the projected trace of the instability is shown in Fig. 17(a). The results are only given for the kriging approach as the ANN results are similar. The clustering of the samples around the instability boundary can be seen. The tracing of the normal modes with altitude changes is presented in Fig. 17(b) at a Mach number of 0.875. The results are shown for the approximation models based on 20 samples and compared to the above reference solution. The agreement between the different approaches is good.

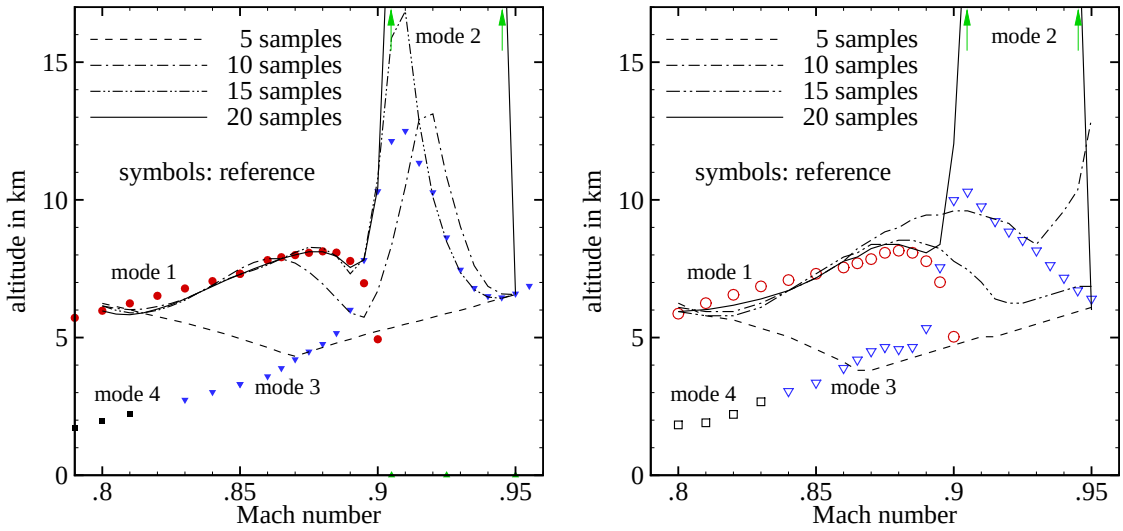

(a) Kriging

(b) ANN

Figure 16. Risk–based sampling for Goland wing/store configuration showing critical values of altitude obtained from approximation models based on kriging and ANN.

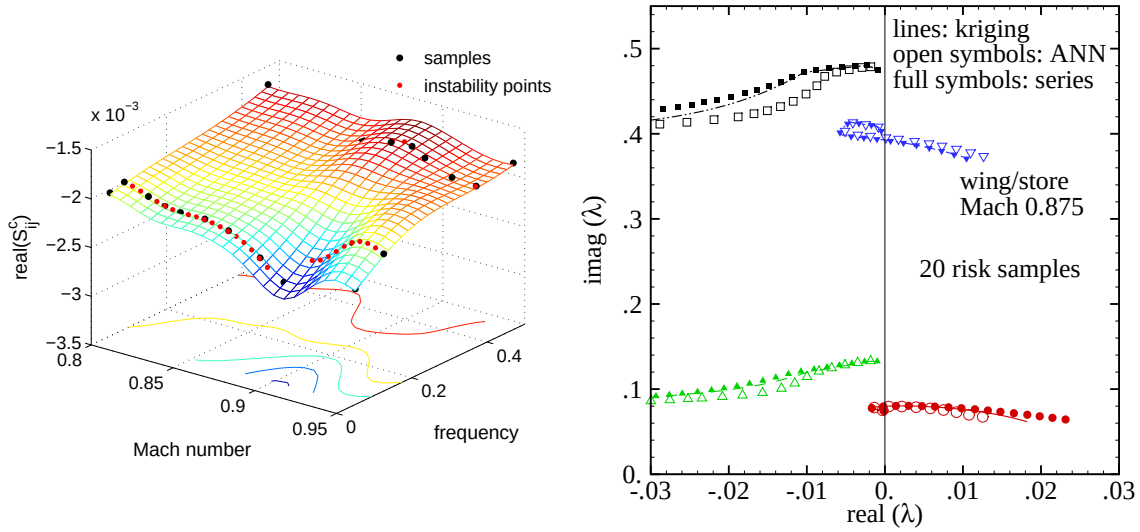

(a) Element real($S^c_{5,2}$) based on 20 samples

(b) Root loci based on 20 samples

Figure 17. Risk–based sampling for Goland wing/store configuration showing (a) representative element of Schur interaction matrix including projected trace of instability for kriging interpolation and (b) root loci at Mach 0.875 for kriging and ANN interpolations compared with reference solution.

The required number of samples correspond to the computational cost of about $20 \times n$ linear solves. Generally, using the series method a total number of $n \times 4n$ linear solves is required to evaluate the series factors per steady state solution to trace all the n wind–off structural modes. Recall that the series factors

are valid only in the vicinity of the chosen shift λ_0, e.g. the normal mode frequencies. Thus, the 20 samples to detect the instability for a range of sub- and transonic freestream Mach numbers using the interpolation methods take about an equivalent cost to predict the instability at one individual Mach number using the series method (which is the most efficient implementation of the full order eigenvalue solver). The savings of the risk–based sampling compared with the grid sampling in Fig. 7 are not significant as the cost reduction is only by a factor of two in this example. This is different for the MDO wing configuration discussed next searching a three dimensional parameter space for instability.

MDO Wing Configuration

The results for the MDO wing configuration, fully accounting for the effects of aerostatic deformation, are shown in Figs. 18 and 19. Figure 18 gives the convergence of the risk–based sampling approach for both the kriging and ANN approximations. Critical values of the altitude are shown for different numbers of samples. Starting from the eight corner samples defining the initial search space, the algorithm converges rapidly and already the second iteration (10 samples) results in an accurate prediction. The problem is converged in less than seven iterations (less than 15 samples) for the kriging formulation to search a three dimensional parameter space for transonic aeroelastic instability. The ANN requires a few more samples for comparable results. As for the Goland wing/store configuration, the observed differences for the risk–based sampling using kriging and ANN are rather small despite the distinct ways to select a new risk–based sample location from intermediate instability points. This emphasises the robustness and generality of the chosen approach.

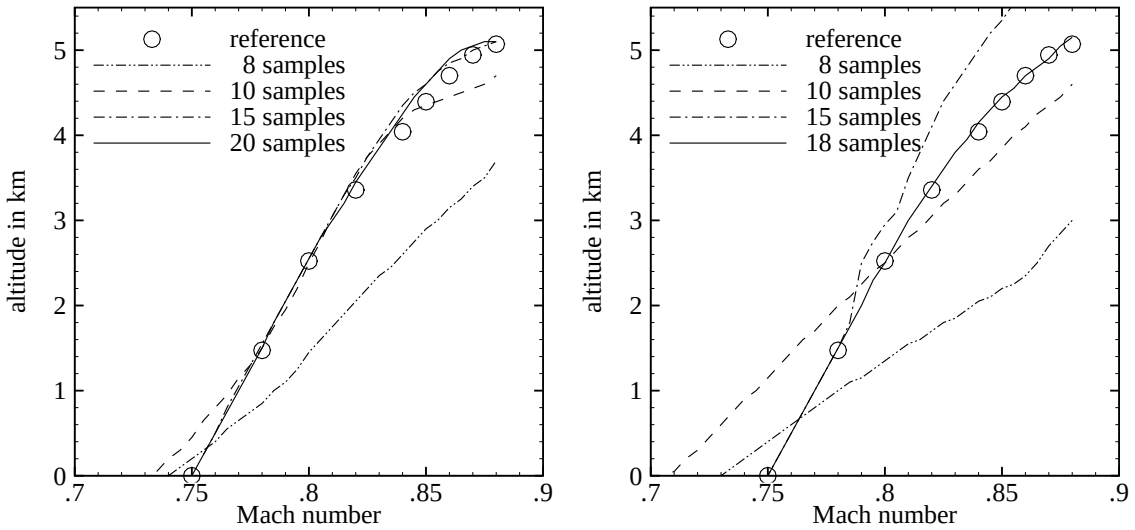

(a) Kriging

(b) ANN

Figure 18. Three dimensional risk–based sampling for MDO wing configuration showing critical values of altitude for interpolations based on kriging and ANN.

The distribution of the samples in the three dimensional parameter space obtained from the kriging approach together with the trace of the first and second mode instabilities is presented in Fig. 19(a). The distribution of samples for the ANN–based search was found to be similar as expected following the Goland results. Comparing the contour slices at Mach 0.8 shown in Figs. 19(a) and 10, it can be seen that the response surface for this representative interaction element is not accurately reproduced globally by the risk–based sampling. This has to be expected considering the very low number of samples. However, locally in the region of the first mode instability, which defines the most critical condition for this configuration focussing the search, the approximation is accurate. The achieved cost reduction is impressive. While the

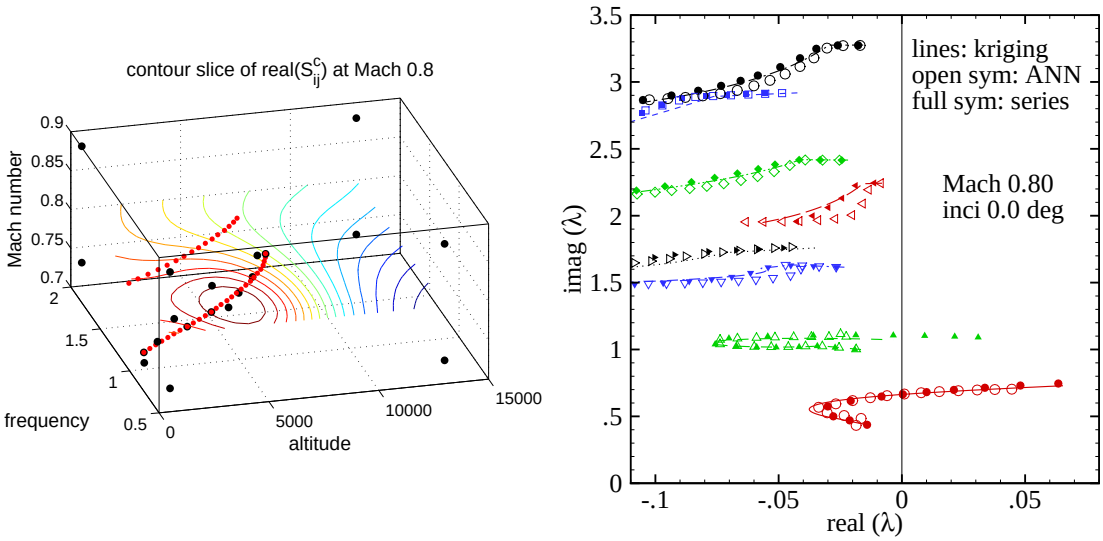

(a) Distribution of 20 risk–based samples

(b) Root loci using risk–based sampling

Figure 19. Three dimensional risk–based sampling for MDO wing configuration showing (a) distribution of 20 samples in parameter space for kriging approach including trace of instability points and (b) mode tracing at Mach 0.8 using approximation models based on 15 samples for kriging and 20 samples for ANN.

grid sampling in Fig. 10 used 252 samples corresponding to the cost of $252 \times n$ linear solves against the large fluid system, about 15 samples are required with the risk–based sampling to detect the instability in the three dimensional search space accurately. This is a cost reduction by a factor of about 20. Recall the requirements when using the series method for the full order eigenvalue solver almost giving a cost reduction by two orders of magnitude.

Importantly, despite concentrating the samples in the region of the most critical conditions, i.e. the first mode instability, leaving large parts of the parameter space essentially uncovered, the mode tracing of the higher frequency modes is not significantly deteriorated. This can be seen in Fig. 19(b) showing the tracing of the modes at Mach 0.8 using the approximation models based on 15 samples for kriging and 20 samples for ANN. A good tracing of the modes compared with the above reference solution can be found. As for the aerofoil case this behaviour can be explained by looking at the governing equations of the structure and the Schur eigenvalue problem. There are two points. First, at high altitudes the influence of the interaction term is relatively small compared with the structural part as the density, defining the bifurcation parameter, is small. Secondly, the higher frequency modes are very insensitive to changes in the interaction matrix elements and the samples of the initial search space already give a good enough approximation. It is clear that the higher the normal mode frequencies are, the more dominant the structural part S^s on the eigenvalue problem becomes. Also, in the figure it is found that the trace of the second mode is not precisely followed. This mode, describing a second instability at lower altitudes compared with the first mode, is subject to a stronger fluid/structure interaction which would require more samples to be represented appropriately. However, the search for all instabilities was not the objective for this demonstration. If the second mode instability describes the most critical condition, then the sampling criterion would place an appropriate sample to correct.

C. Summary for Instability Searches

The aeroelastic stability analysis based on the approximation of the interaction matrix is very efficient as repeated operations on the full order fluid system are avoided. The limiting factor in using either of the two

discussed approximation formulations (kriging and ANN) is the construction of the surrogate model itself as this step requires exact numerical samples to represent the physics described by the interaction matrix. In this preceding section the sampling is tailored for the aeroelastic stability analysis instead to reduce the required number of expensive evaluations.

For the instability search, it was found to be useful to start from an initial small set of samples defining the corners of the parameter space, and to run complete stability analyses with the intermediate approximation models which is possible due to the very low computational cost. New sample locations are chosen according to high risk of finding an instability, i.e. at intermediate instability points. This approach exploits the characteristics of the aeroelastic stability problem as globally accurate approximations of the interaction matrix elements are not required. Low values of the independent parameter result in a dominant structural eigenvalue problem, whereas higher values give a stronger fluid/structure interaction demanding a better approximation which is achieved by placing samples accordingly. For the presented test cases, the risk–based sampling converges the instability boundary in a few iterations while significant differences between the two interpolation techniques are not observed.

6. Conclusions

The use of interpolation techniques, namely kriging and artificial neural networks, in routine transonic aeroelastic stability analyses applying high fidelity computational fluids dynamics, currently the Euler equations, has been presented. The Schur complement eigenvalue formulation solves a small nonlinear eigenvalue problem for the structural system which is corrected by the aerodynamic influence. As the evaluation of this aerodynamic influence is computationally very demanding, thus limiting the approach when applied for large scale analyses, its approximation based on interpolating exact numerical samples to represent the fluid response is discussed.

The approximation approach for the two interpolation techniques is demonstrated for a two degrees–of–freedom NACA 0012 aerofoil configuration and two wing cases including the Goland wing/store and MDO wing configurations. Accurate results are found throughout compared with the exact eigenvalue solver at very competitive cost. Additionally, the approximation approaches are exploited to search larger parameter spaces for aeroelastic instability, while assuming little prior knowledge of the configuration, by using an efficient coordinated risk–based sampling where new samples are placed iteratively at the locations of intermediate instability points, i.e. at locations of high risk. The approach converges rapidly for the presented test cases resulting in a further cost reduction compared with the basic, brute–force, grid sampling approach to cover the parameter space. Importantly, the stability predictions are rather insensitive to the chosen interpolation tool, herein kriging and artificial neural networks, and the results do not suggest a preferred option.

Acknowledgments

This research forms part of the programme of the Marie Curie Excellence Team "Ecerta" supported by the European Union under contract MEXT–CT–2006–042383.

References

[1] Garrick, I. E. and Reed III, W. H., "Historical development of aircraft flutter," *Journal of Aircraft*, Vol. 18, No. 11, 1981, pp. 897–912.

[2] Bunton, R. W. and Denegri, Jr., C. M., "Limit cycle oscillation characteristics of fighter aircraft," *Journal of Aircraft*, Vol. 37, No. 5, 2000, pp. 916–918.

[3] Dowell, E. H., Edwards, J. W., and Strganac, T. W., "Nonlinear aeroelasticity," *Journal of Aircraft*, Vol. 40, No. 5, 2003, pp. 857–874.

[4] Hassig, H. J., "An approximate true damping solution of the flutter equation by determinant iteration," *Journal of Aircraft*, Vol. 8, No. 11, 1971, pp. 885–889.

[5] Albano, E. and Rodden, W. P., "A doublet–lattice method for calculating lift distributions on oscillating surfaces in subsonic flows," *AIAA Journal*, Vol. 7, No. 2, 1969, pp. 279–285.

[6] Lucia, D. J., Beran, P. S., and Silva, W. A., "Reduced–order modeling: new approaches for computational physics," *Progress in Aerospace Sciences*, Vol. 40, 2004, pp. 51–117.

[7] Silva, W. A. and Bartels, R. E., "Development of reduced–order models for aeroelastic analysis and flutter prediction using the CFL3Dv6.0 code," *Journal of Fluids and Structures*, Vol. 19, 2004, pp. 729–745.

[8] Romanowski, M. C., "Reduced order unsteady aerodynamics and aeroelastic models using Karhunen–Loeve eigenmodes," *AIAA Paper 96–3981*, 1996.

[9] Hall, K. C., Thomas, J. P., and Dowell, E. H., "Proper orthogonal decomposition technique for transonic unsteady aerodynamic flows," *AIAA Journal*, Vol. 38, No. 10, 2000, pp. 1853–1862.

[10] Lieu, T., Farhat, C., and Lesoinne, M., "Reduced–order fluid/structure modeling of a complete aircraft configuration," *Comput. Methods Appl. Mech. Engrg.*, Vol. 195, 2006, pp. 5730–5742.

[11] Morton, S. A. and Beran, P. S., "Hopf–bifurcation analysis of airfoil flutter at transonic speeds," *AIAA Paper 96–0060*, 1996.

[12] Morton, S. A. and Beran, P. S., "Hopf bifurcation analysis applied to deforming airfoils at transonic speeds," *AIAA Paper 97–1772*, 1997.

[13] Morton, S. A. and Beran, P. S., "Hopf–bifurcation analysis of airfoil flutter at transonic speeds," *Journal of Aircraft*, Vol. 36, No. 2, 1999, pp. 421–429.

[14] Badcock, K. J., Woodgate, M. A., and Richards, B. E., "Hopf bifurcation calculations for a symmetric airfoil in transonic flow," *AIAA Journal*, Vol. 42, No. 5, 2004, pp. 883–892.

[15] Badcock, K. J., Woodgate, M. A., and Richards, B. E., "Direct aeroelastic bifurcation analysis of a symmetric wing based on Euler equations," *Journal of Aircraft*, Vol. 42, No. 3, 2005, pp. 731–737.

[16] Woodgate, M. A. and Badcock, K. J., "Fast prediction of transonic aeroelastic stability and limit cycles," *AIAA Journal*, Vol. 45, No. 6, 2007, pp. 1370–1381.

[17] Badcock, K. J. and Woodgate, M. A., "Bifurcation prediction of large–order aeroelastic models," *AIAA Journal*, Vol. 48, No. 6, 2010, pp. 1037–1046.

[18] Marques, S., Badcock, K. J., Khodaparast, H. H., and Mottershead, J. E., "CFD based aeroelastic stability predictions under the influence of structural variability," *AIAA Paper 2009–2324*, 2009, to appear in Journal of Aircraft.

[19] Timme, S. and Badcock, K. J., "Searching for transonic aeroelastic instability using an aerodynamic model hierarchy," *AIAA Paper 2010–3048*, 2010.

[20] Timme, S., Marques, S., and Badcock, K. J., "Transonic aeroelastic stability analysis using a kriging–based Schur complement formulation," 2010, To be presented at the AIAA Atmospheric Flight Mechanics Conference, Toronto, Canada, 2010.

[21] Badcock, K. J., Richards, B. E., and Woodgate, M. A., "Elements of computational fluid dynamics on block structured grids using implicit solvers," *Progress in Aerospace Sciences*, Vol. 36, 2000, pp. 351–392.

[22] Osher, S. and Chakravarthy, S. R., "Upwind schemes and boundary conditions with applications to Euler equations in general geometries," *Journal of Computational Physics*, Vol. 50, 1983, pp. 447–481.

[23] van Leer, B., "Towards the ultimative conservative difference scheme. V. a second–order sequel to Godunov's method," *Journal of Computational Physics*, Vol. 32, 1979, pp. 101–136.

[24] Jameson, A., "Time dependent calculations using multigrid with applications to unsteady flows past airfoils and wings," *AIAA Paper 91–1596*, 1991.

[25] Fung, Y. C., *An introduction to the theory of aeroelasticity*, John Wiley & Sons, Inc., New York, NY, 1955.

[26] Taylor, N. V., Allen, C. B., Gaitonde, A. L., Jones, D. P., Vio, G. A., Cooper, J. E., Rampurawala, A. M., Badcock, K. J., Woodgate, M. A., and de C. Henshaw, M. J., "Aeroelastic analysis through linear and non–linear methods: a summary of flutter prediction in PUMA DARP," *The Aeronautical Journal*, Vol. 110, No. 1107, 2006, pp. 333–343.

[27] Wright, J. R. and Cooper, J. E., *Introduction to aircraft aeroelasticity and loads*, John Wiley & Sons, Ltd, Chichester, England, 2007.

[28] Bekas, C. and Saad, Y., "Computation of smallest eigenvalues using spectral schur complements," *SIAM J. Sci. Comput.*, Vol. 27, No. 2, 2005, pp. 458–481.

[29] Bakhle, M. A., Mahajan, A. J., Keith, , Jr., T. G., and Stefko, G. L., "Cascade flutter analysis with transient response aerodynamics," *Computers & Structures*, Vol. 41, No. 5, 1991, pp. 1073–1085.

[30] Silva, W. A., "Simultaneous excitation of multiple–input/multiple–output CFD–based unsteady aerodynamic systems," *Journal of Aircraft*, Vol. 45, No. 4, 2008, pp. 1267–1274.

[31] Jones, D. R., Schonlau, M., and Welch, W. J., "Efficient global optimization of expensive black–box functions," *Journal of Global Optimization*, Vol. 13, No. 4, 1998, pp. 455–492.

[32] Sacks, J., Welch, W. J., Mitchell, T. J., and Wynn, H. P., "Design and analysis of computer experiments," *Statistical Science*, Vol. 4, No. 4, 1989, pp. 409–435.

[33] Lophaven, S. N., Nielsen, H. B., and Sœndergaard, J., "DACE – A matlab kriging toolbox," Tech. Rep. IMM–TR–2002–12, Technical University of Denmark, Denmark, 2002.

[34] Krose, B. and van der Smagt, P., *An introduction to neural networks*, The University of Amsterdam, Amsterdam, The Netherlands, 8th ed., 1996.

[35] Rodden, W. P. and Johnson, E. H., *MSC.Nastran aeroelastic analysis user's guide*, MSC.Software Corporation, Santa Ana, CA, 2004.

[36] McDevitt, J. B. and Okuno, A. F., "Static and dynamic pressure measurements on a NACA 0012 airfoil in the Ames high Reynolds number facility," Tech. Rep. NASA–TP–2485, Ames Research Center, Moffett Field, CA, 1985.

[37] Beran, P. S., Khot, N. S., Eastep, F. E., Snyder, R. D., and Zweber, J. V., "Numerical analysis of store–induced limit–cycle oscillation," *Journal of Aircraft*, Vol. 41, No. 6, 2004, pp. 1315–1326.

[38] Goura, G. S. L., *Time marching analysis of flutter using computational fluid dynamics*, Ph.D. thesis, Department of Aerospace Engineering, University of Glasgow, Glasgow, United Kingdom, 2001.

[39] Swift, A. and Badcock, K. J., "Inter–grid transfer influence on transonic flutter predictions," *AIAA Paper 2010–3049*, 2010.